CHAPTER 4

OBSERVATIONS

4.1 CONTINUUM OBSERVATIONS

This chapter describes continuum observations made using the digital receiver system. Details of antenna measurements, calibration and data processing are described here. At the end of the chapter some continuum maps are presented.

4.2 ANTENNA MEASUREMENTS

1. The phase shifters in the N-S array were originally made for 30 MHz. The present observations are carried out at 34.5 MHz. Thus it was found essential to measure the actual phase shifts introduced by the phase shifters at 34.5 MHz. All the 135 phase shifts in the field were measured. Their average and R.M.S. variations were noted. The variation in the phase shift values cause different interferometers to have different primary beams. The beam shapes of all the interferometer elements were calculated for different phase shifter settings. From the peak down to 3 dB points the beams of different interferometers have gain

variations (n) less than ±0.5 dB (R.M.S). R.M.S variations increase to ±3 dB at 20 dB points. The average primary beam of the 23 interferometers is used for synthesis. This results in errors in the map. Since 23 interferometers are used for the synthesis, the error will be $n/\sqrt{23}$.

The grading of the antenna was also measured. The N-S grading in any group of four dipoles was found to be uniform within a random error of ±1dB (R.M.S). The E-W grading was also found to be uniform with a random fluctuation of ±1.5 dB.

2. It was confirmed that the sky background noise dominates the system noise in both N-S and E-W interferometer elements. In the N-S array this was done by terminating the inputs of the FET preamplifiers of the interferometer elements with 75 Ω and recording the total power output of an interferometer element on a chart recorder. The dipoles were then connected to the preamplifier and the deflection on the chart was noted again. This was atleast 10dB more than the deflection when the amplifier was terminated (even when the interferometer element was phased to point to the coldest regions of the sky). Thus the sky noise is at least 10 times more than the receiver noise. In the E-W, the total power output with and without FET amplifiers cannot be measured since there are 160 FET amplifiers in this element of the interferometer. Since the F.E.T. amplifiers used in the E-W and the N-S array are same, the same minimum factor of 10 for the ratio

of sky to receiver temperature can be assumed. These tests ensure that the sky noise and not the receiver noise limits the minimum detectable flux, which therefore varies with the position of the sky, as does the sky brightness.

3. To decide the dynamic range of the input to the Z.C.D., the antenna (4 x 4) was phased to the Galactic Centre and the Galactic pole, which are the brightest and coldest regions in the sky. Total power deflections were noted down on a chart as the sky drifted for more than one hour in each case. The deflections differed by 6 dB. Having measured this, it was ensured that the Z.C.D. at least sees a 400 mv peak to peak noise voltage at its input at all times.

4. The output of each interferometer is brought to the lab on openwire transmission lines. Day and night temperatures at Guaribidanur can be different by 10° F. The phase variation of the lines with time over a day was measured by feeding a CW signal. The phase fluctuations were found to be less than 3°. This fitted well with the estimates made by using the linear coefficient of expansion of the material of the transmission line (copper).

5. The Gaussian nature of the noise received by the antenna was confirmed by using the threshold detectors. The four threshold detectors were calibrated by feeding C.W. of known amplitude. Then, the noise of the antenna was fed to the threshold detectors. The σ of the noise was

determined by assuming Gaussian statistics. σ was found to be independent of the threshold used, indicating the gaussian nature of the noise.

6. Since the E-W array is 1.5 kms long and the N-S array is only 500 m long, the signal from the E-W array is grossly delayed before reaching the lab. To compensate for this, the signal from the N-S interferometers is delayed by 64 clock periods before reaching the correlator. Since this is in excess of what is required, the E-W signal has to be delayed in the lab for maximising the correlation. The actual delay required was measured, by feeding the same noise signal to two dipoles, one in the E-W and another in the N-S array. Cross correlation of the signals received in the lab were measured for different delay settings of the variable delay sampler (Section 3.6.1). The figure (4.1) shows the correlations as a function of the delay. The correlation maximises when the E-W signal is delayed by 56 clock periods (when the clock period is 0.5 μsecs.). Thus the E-W signal has to be delayed 4 μsecs less than the N-S signal in the lab which is exactly what is expected from the greater length of the E-W array.

4.3 INTERFEROMETER PRIMARY BEAMS

Figure 4.2 shows the primary beam positions in which observations were carried out. It shows the resultant beam obtained by multiplying the primary beam (voltage pattern) of any one of the N-S interferometer elements with that of

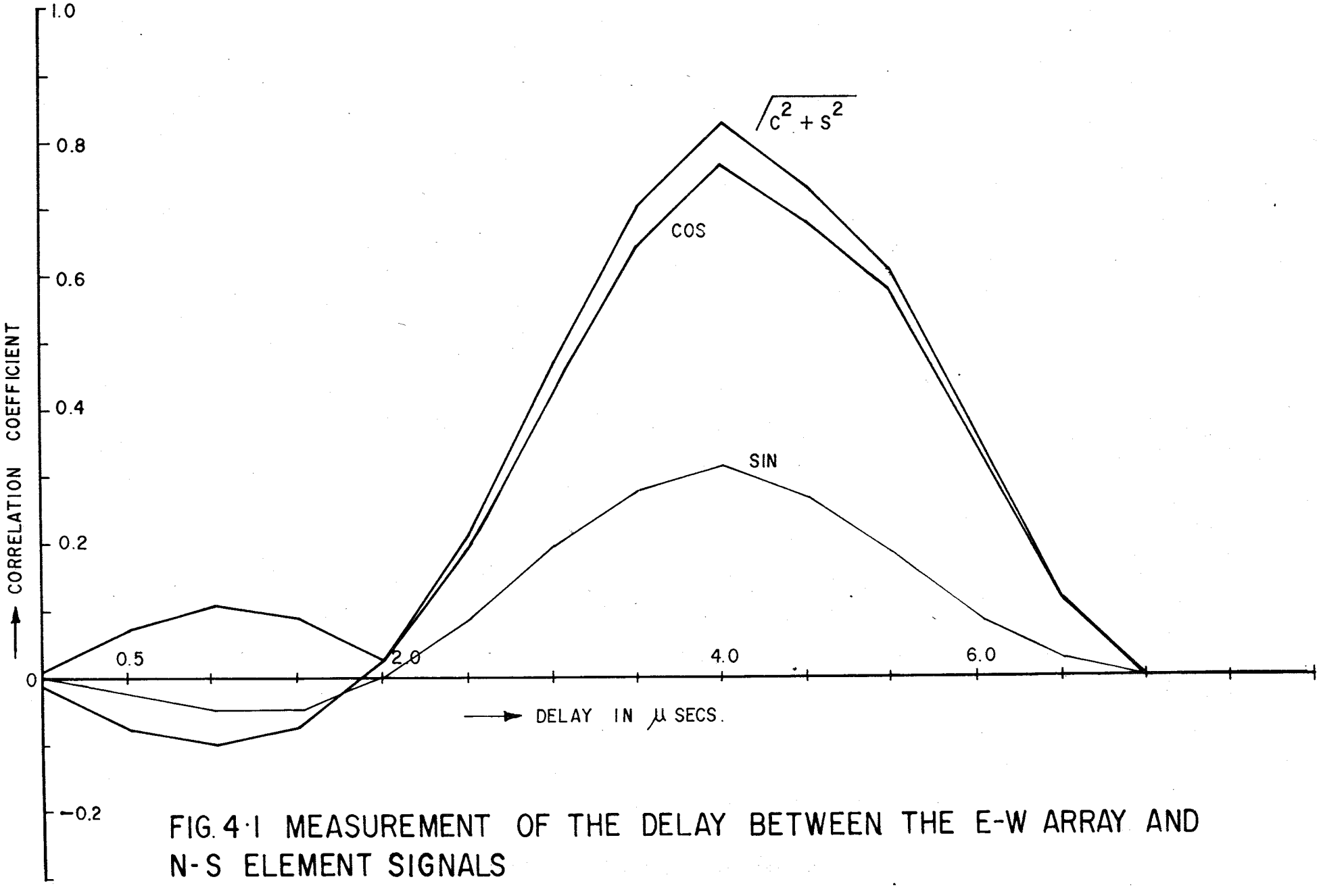

FIG. 4·1 MEASUREMENT OF THE DELAY BETWEEN THE E-W ARRAY AND N-S ELEMENT SIGNALS

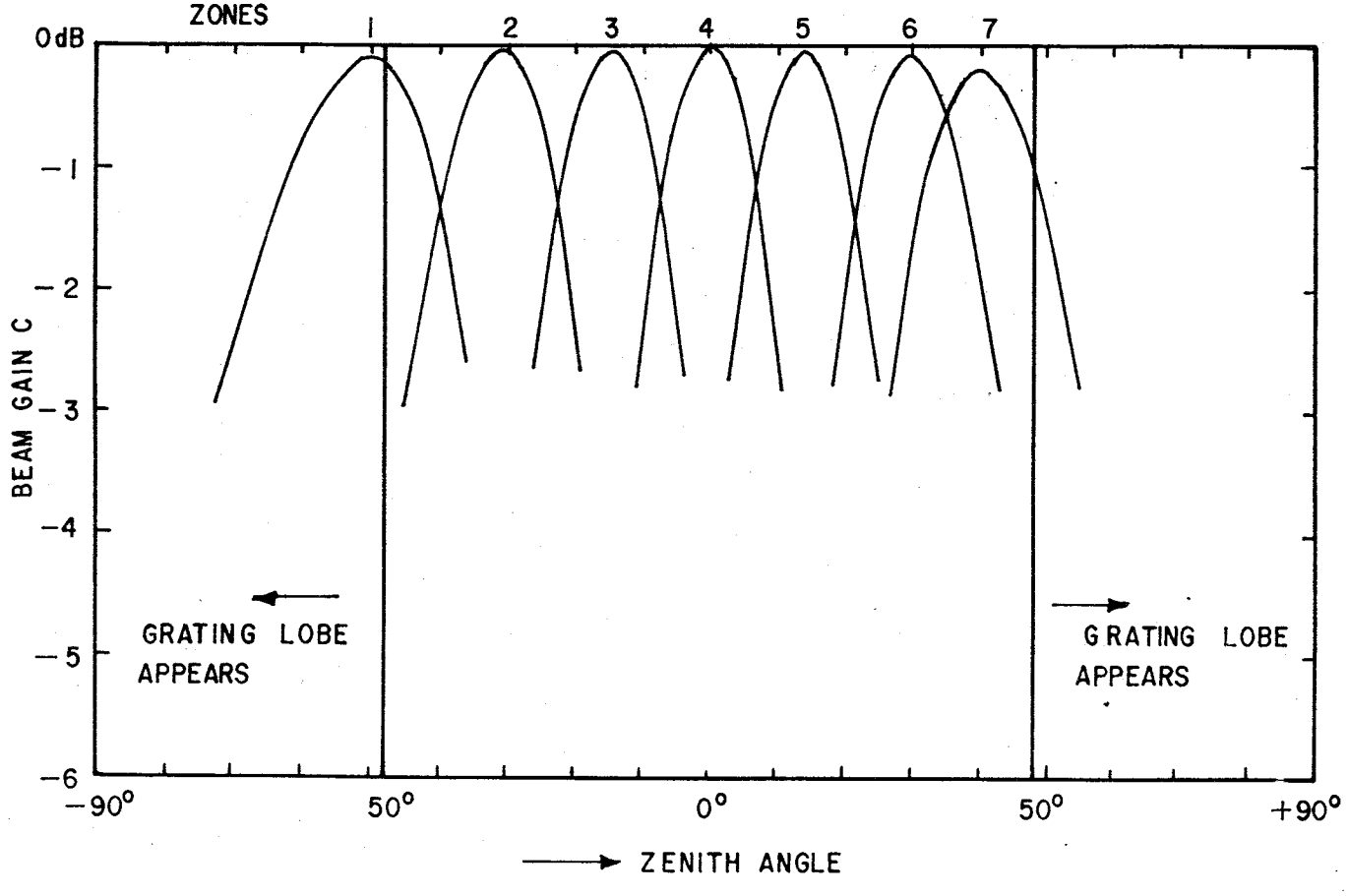

PHASE SHIFTER SETTINGS.

	E-W		N-S	
	ϕ_1	ϕ_2	ϕ_1	ϕ_2
1	169	332	157	299
2	113	217	106	204
3	56	115	51	95
4	0	0	0	0
5	323	269	310	249
6	266	167	255	140
7	210	115	204	95

(IN DEGREES)

FIG. 4·2 INTERFEROMETER PRIMARY BEAM POSITIONS.

the E-W array in the N-S direction. The 1st and 2nd level phase shifter settings in the N-S and E-W array are indicated. These seven beams are the ones in which the 2nd level phase shifter setting ϕ_2 is very nearly equal to twice the 1st level phase shifter setting ϕ_1. When $\phi_2 \neq 2\phi_1$, the resultant beam will be broader and will have less gain at the centre of the beam. Some of the beams shown in the figure do not have unity gain at the centre of the beam since the phase shifters in the E-W and N-S arrays are not exactly identical. Even though the seven beams span the observable region of the sky without grating lobes ($\pm 50^{\circ}$ of the zenith), it is not possible to synthesize the entire sky due to the following limitation.

We are measuring the complex correlation coefficients between the E-W and various elements of the N-S array. These complex coefficients are called visibilities. They are obtained for various N-S baselines from 0 to 480 metres in steps of 20 metres. Such a sampling restricts the primary beam size for synthesis with acceptable sidelobe levels. The visibility and the brightness distribution are related by a Fourier Transform relation. By the sampling theorem, when the visibilities are spaced 20 mts (2.3λ) apart the field of view should be restricted to $1/2 \times 2.3\lambda = 12^{\circ}.45$. But the main beam of each interferometer has an extent of $24^{\circ}.9$ between nulls. For this extent of the main beam, the visibilities should have been measured at intervals of 10 mts. Thus the visibilities are undersampled

by a factor of 2. This undersampling restricts the field of view that can be synthesized for each primary beam position. In an array like the one in Gauribidanur, if dipoles are combined in the field, sampling requirement cannot be satisfied unless successive interferometers have overlapping dipoles. For this 90 elements should be combined to obtain 45 interferometers each having four rows.

Note: The situation is very similar to non-overlapping box- car averaging of time series. Let $t_1, t_2, \ldots, t_n$ be Nyquist samples of a time series spaced t secs apart (Refer Fig. 4.3). Let a new time series $t'_1, t'_2, \ldots t'_n$ be generated from this series where $t'_1 = t_1 + t_2 + t_3 + t_4$, $t'_2 = t_5 + t_6 + t_7 + t_8 \ldots\ldots$ This averaging changes the power spectrum. The resulting new spectrum is shown in figure. This is not bandlimited in the strict sense. This new time series should have samples separated in time by atleast 2t secs for reconstruction of the main portion of the power spectrum without aliasing. But the new time series has samples separated in time by 4t seconds. Thus for the new power spectrum time series should be $T_1, T_2, \ldots T_n$ where $T_1 = t_1 + t_2 + t_3 + t_4$; $T_2 = t_3 + t_4 + t_5 + t_6$; ...

To fix the extent of each primary beam that can be synthesized, the synthesized beam can be thought of as obtained by multiplying an array factor with the primary beam of each interferometer. This array factor is of an array whose interferometers are spaced 20 mtrs apart. Most

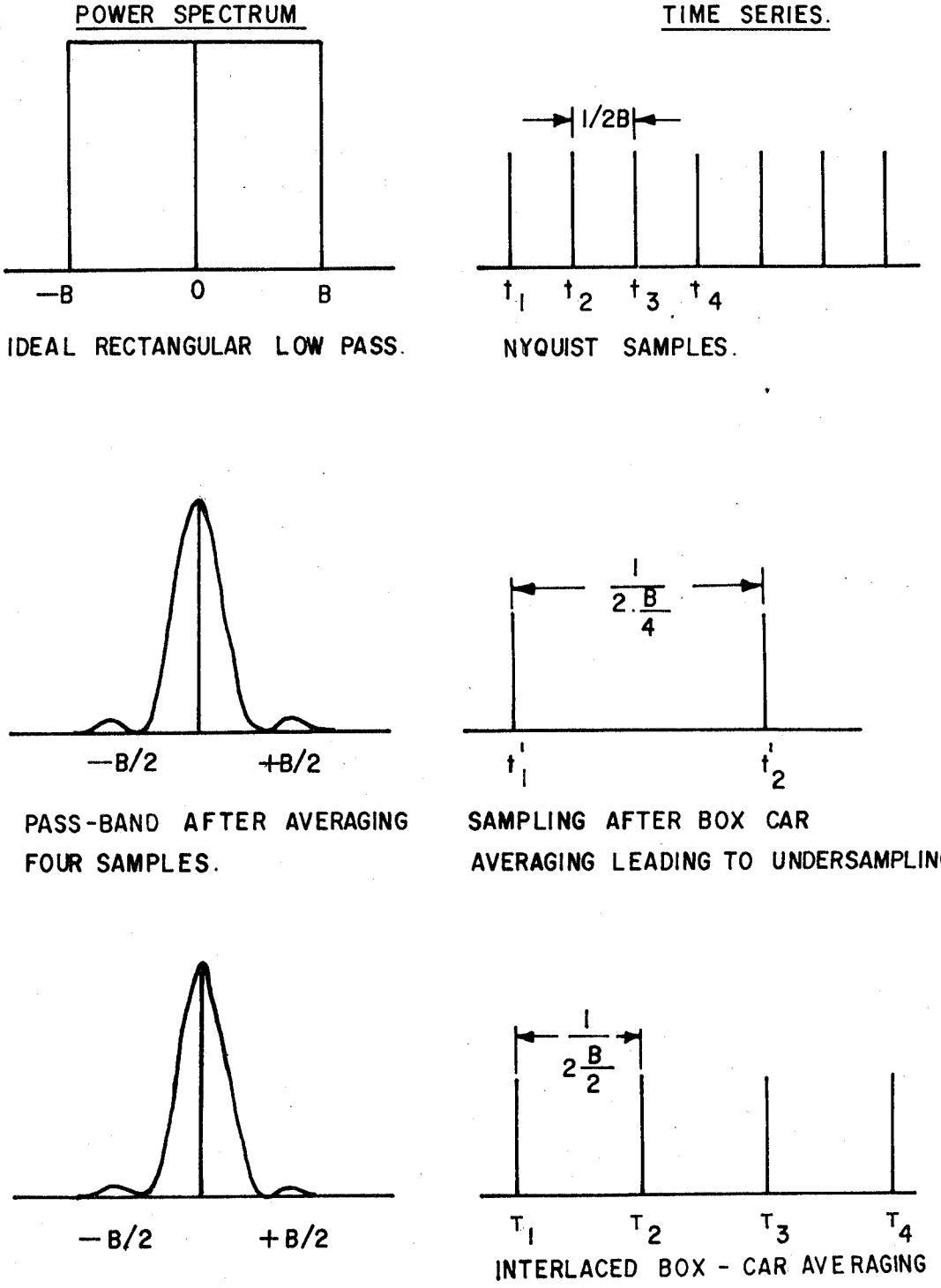

FIG. 4·3 BOX - CAR AVERAGING.

important characteristic of its pattern will be that at 34.5 MHz it will have 4 or 5 grating lobes depending on the zenith angle to which array is phased.

Let us consider the zenith beam. ($\phi_{1NS} = \phi_{2NS} = \phi_{1EW} = \phi_{2EW} = 0$). For the synthesized beam at the zenith, the array factor and the primary beam shape are as shown in figure 4.4. The synthesized beam which will be the product of the two patterns shown will be acceptable as it has no grating responses. The array factor and the primary beam for the synthesized beam at a zenith angle = 12°.5 is as shown in Fig. 4.5. The synthesized beam will be unacceptable as it has two main beams. As one moves towards the zenith, the primary beam response attenuates one of the grating lobes. Considering around 10 dB suppression of grating lobes as acceptable for synthesis, Table 4.1 lists the zenith angle extent that can be mapped by different primary beams. Since the N-S array has a spacing of 5 mtrs $> \lambda_{34.5}/2$ grating lobes appear for zenith angle $> 48^{\circ}$. For zenith angle = 60°, there are two equal main beams irrespective of the beam forming technique. Thus the following regions cannot be synthesized by the 7 primary beams.

1. Regions beyond -48° to $+48^{\circ}$ zenith angle

2. Regions between -5° to -10°, $+5^{\circ}$ to $+10^{\circ}$, $+20^{\circ}$ to $+23^{\circ}$, -20° to -25° zenith angle.

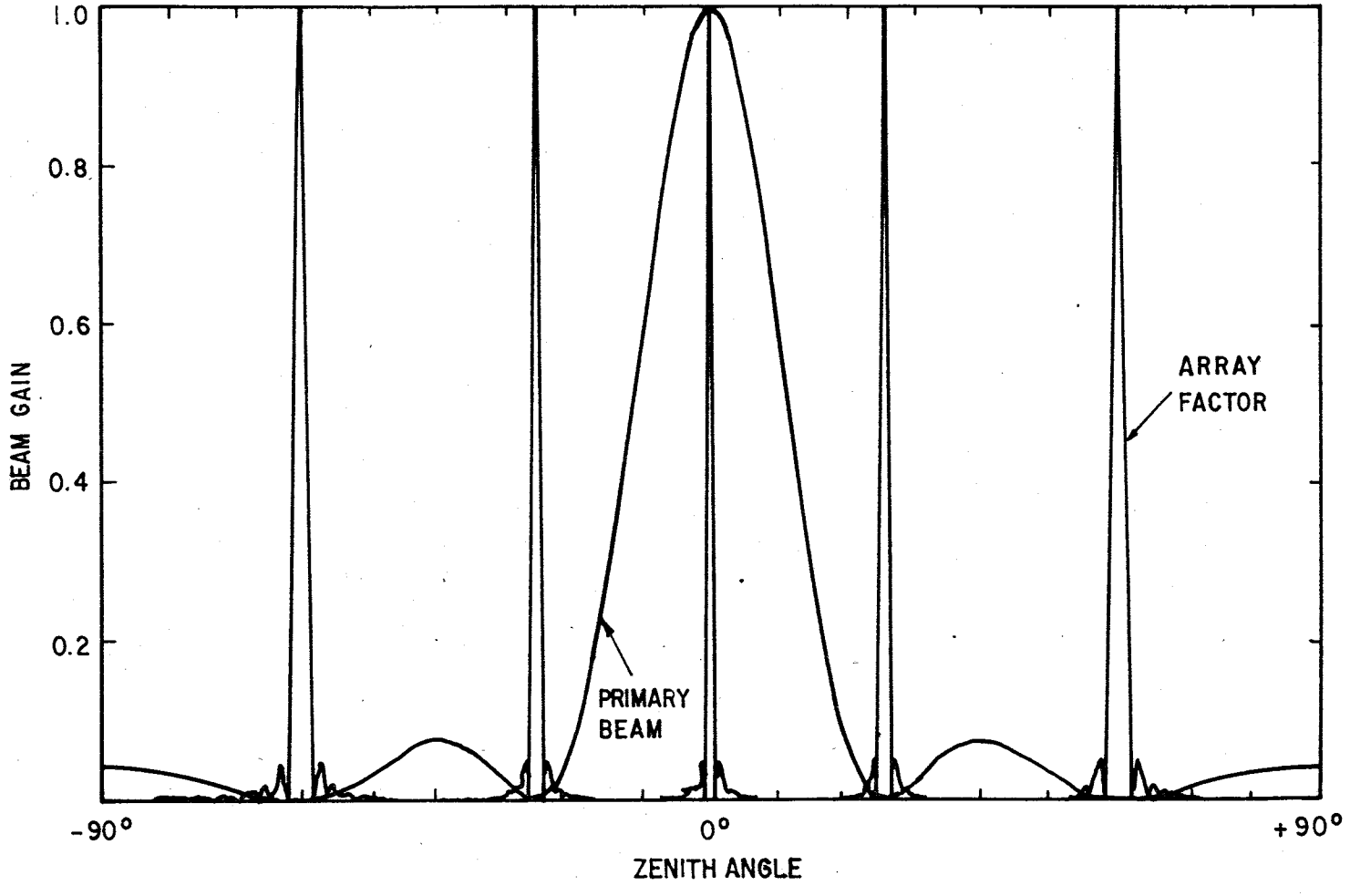

FIG.4·4 PRIMARY BEAM AND ARRAY FACTOR FOR THE SYNTHESIZED BEAM AT ZENITH.

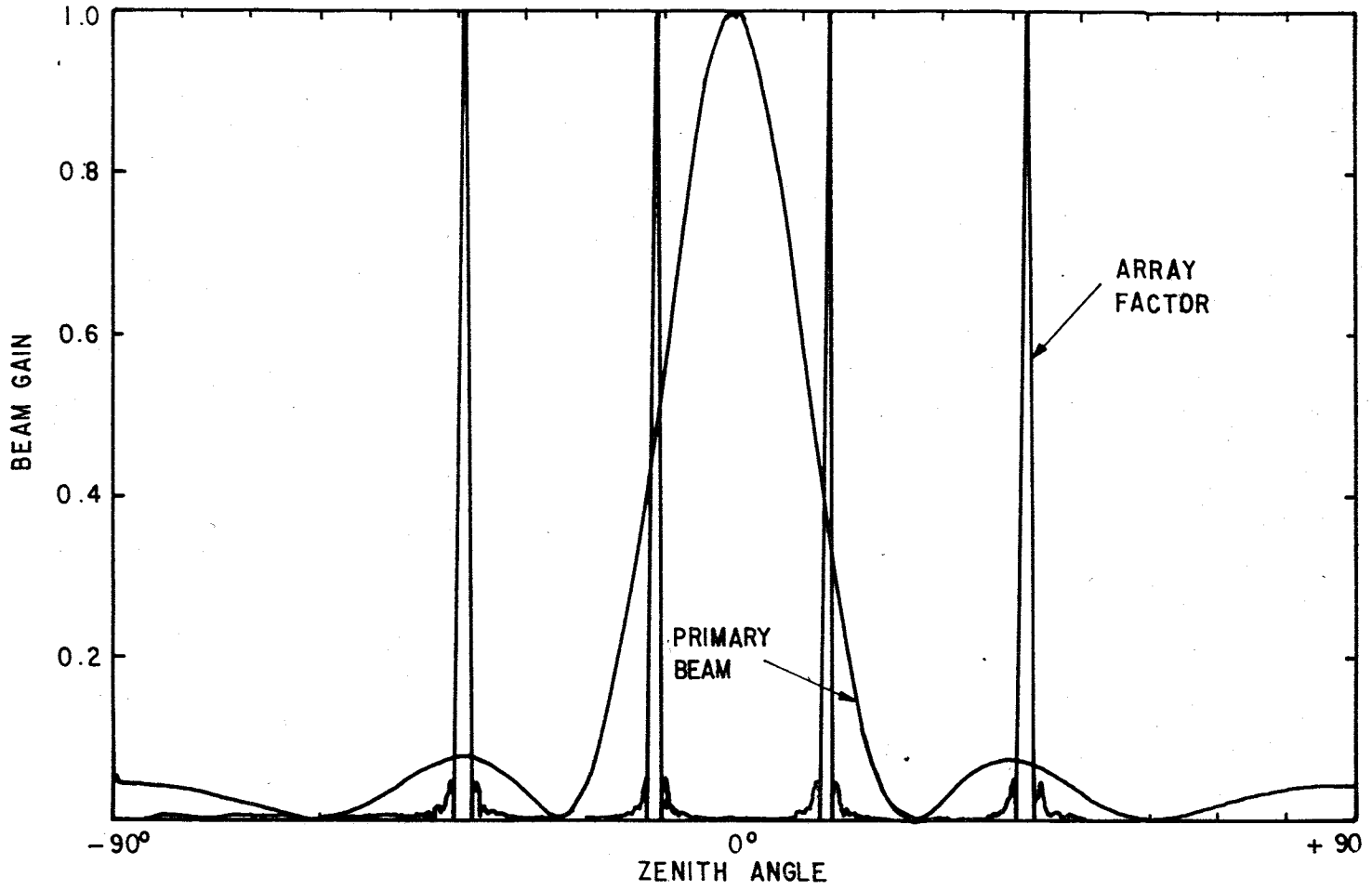

FIG.4·5 PRIMARY BEAM AND ARRAY FACTOR FOR THE SYNTHESIZED BEAM AWAY FROM ZENITH.

Primary beam numbers (Fig. 4.2)	Zenith Angle Extent that can be mapped
1	-48° to -35°
2	-37° to -25°
3	-20° to -10°
4	-5° to $+5^{\circ}$
5	23° to 36°
7	32° to 48°

TABLE 4.1 ZENITH ANGLE EXTENT THAT CAN BE MAPPED BY DIFFERENT PRIMARY BEAMS.

To map these regions one has to use more primary beam positions. Alternatively, knowing the brightness distribution of the region where the grating lobes fall, the brightness distribution of these regions can be solved.

4.4 DELAY COMPENSATION FOR DIFFERENT PRIMARY BEAM POSITIONS

The difference in the arrival time of a wave front between E-W array and various interferometers increases with the spacing and zenith angle. If this delay is not compensated, it causes bandwidth decorrelation. The facility exists in the correlators to delay the E-W or N-S signals for observations of Northern or Southern zenith angles. Delay steps are restricted to integral multiples of clock periods and a maximum of 3 clock periods delay can be obtained. Due to hardware limitations, the same delay has to be set for groups of four interferometers. Thus there are 6 groups and 7 zones (for different primary beam positions). Figure 4.6 shows the delay settings for each zone and the uncompensated delay for the centre of the beam in various interferometers. The R.M.S. uncompensated delay is .169 μsecs . This hardly causes any bandwidth decorrelation in a DSB system with an R.F. bandwidth of about 400 KHz, where the final videoband is only half the R.F. bandwidth. A DSB system has the additional advantage that the phase calibration is independent of the delay settings.

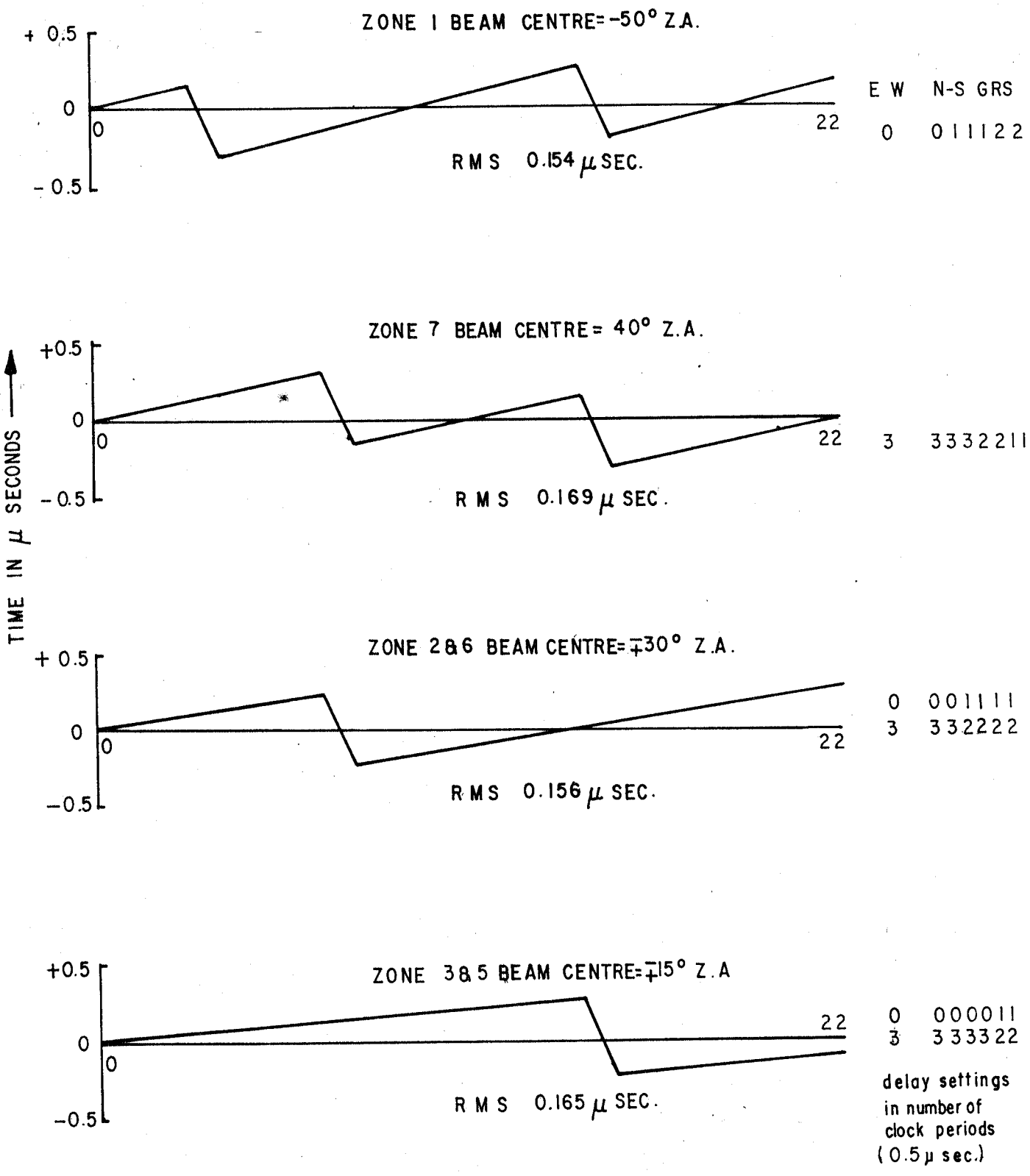

FIG. 4·6 UNCOMPENSATED DELAY FOR DIFFERENT INTERFEROMETERS AT BEAM CENTRES.

4.5 DATA COLLECTION

Observations in each zone have been carried out for 18 to 19 hours.

1. Antenna and receiver system checks were performed before observations in each zone. Sample dipoles (at random) in each group of the E-W and N-S array were also tested. This was done by feeding a known amount of noise to the dipole and the deflection due to it was measured on a chart recorder in the lab. IF noise levels of the superheterodyne receivers were monitored on an oscilloscope. The receiver system in the lab can be easily checked by switching off the antenna and connecting C.W. and/or noise to the system. Correlation values can be obtained on the printer and any malfunction can be attended to.

2. Before observations, the phase shifters were set to the required values. Delay settings appropriate to each zone were ensured.

3. Recording is enabled by a push button on the M.T. interface. It commences at the beginning of a sidereal minute, and the recording sequence was as follows:

a) First the M.T.I. acquires timing information from the astronomical clock and writes a header of 12 bytes on M.T. and writes an E.O.R.. The 12 bytes are

2 bytes - 4 digits of Julian Day

1 byte - hours

1 byte - Mts

1 byte - secs

1 byte - zone setting

3 bytes - delay setting

3 bytes - sampling clock used, integration time, E-W bandwidth used and L.O. frequency.

b) After the acquisition of the time, 64 bytes of information are written after each integration time. For the present observations, the maximum permissible integration time, bandwidth and sampling frequency which are 256 msecs, 400 KHz and 2 MHz respectively were used. The 64 bytes represent 23 complex correlation coefficients, 8 total power outputs and 1 dummy byte. The total power of each channel requires only the cosine correlator output. But once a channel is chosen, the hardware writes both the cosine and sine correlator outputs on the M.T. Thus out of 64, only 56 bytes contain useful information. The dummy data (all 1's) helps to identify channel numbers during data processing. Any recording error can be noticed immediately. In 30 preintegration periods, 1920 bytes of data are written on magnetic tape. At the end of this, a record gap is written. This amounts approximately to a record written each 8 seconds. The record gap insertion takes about 0.7 secs. Just before the end of each sidereal hour a calibration is recorded as follows. The E.O.R. pulse after 59 mts 30 secs of a sidereal hour switches off the E-W antenna and the 4 x 4 N-S element used for the total power

measurement. It then switches on noise diodes in the field. One full record of calibration data is written on the M.T., and at the end of the calibration , the E.O.F. circuit is actuated and a file gap is written after which the recording stops. Recording commences again at the beginning of the next sidereal hour with the acquisition of time.

4. In the event of power failure, the M.T.U. and its interface switch over to the battery supply. A record gap followed by a file gap are immediately written. When the A.C. power returns, recording starts at the beginning of a new sidereal minute with time acquisition.

5. After every recording session the antennna is switched off and CW/NG in the lab is switched on. 8 to 10 records of information are written on magnetic tape. Phase drifts and channel failures can be identified from these records. It is proposed in the future to record this automatically at the end of each hour for one record length.

4.6 DATA PROCESSING

The flow chart for data processing is shown in figures 4.7A,B and C.

1. Data Transfer

The data recorded on magnetic tape is transferred to the computer. Data transfer and analysis are done on one hour blocks of data recorded in different files. Each file

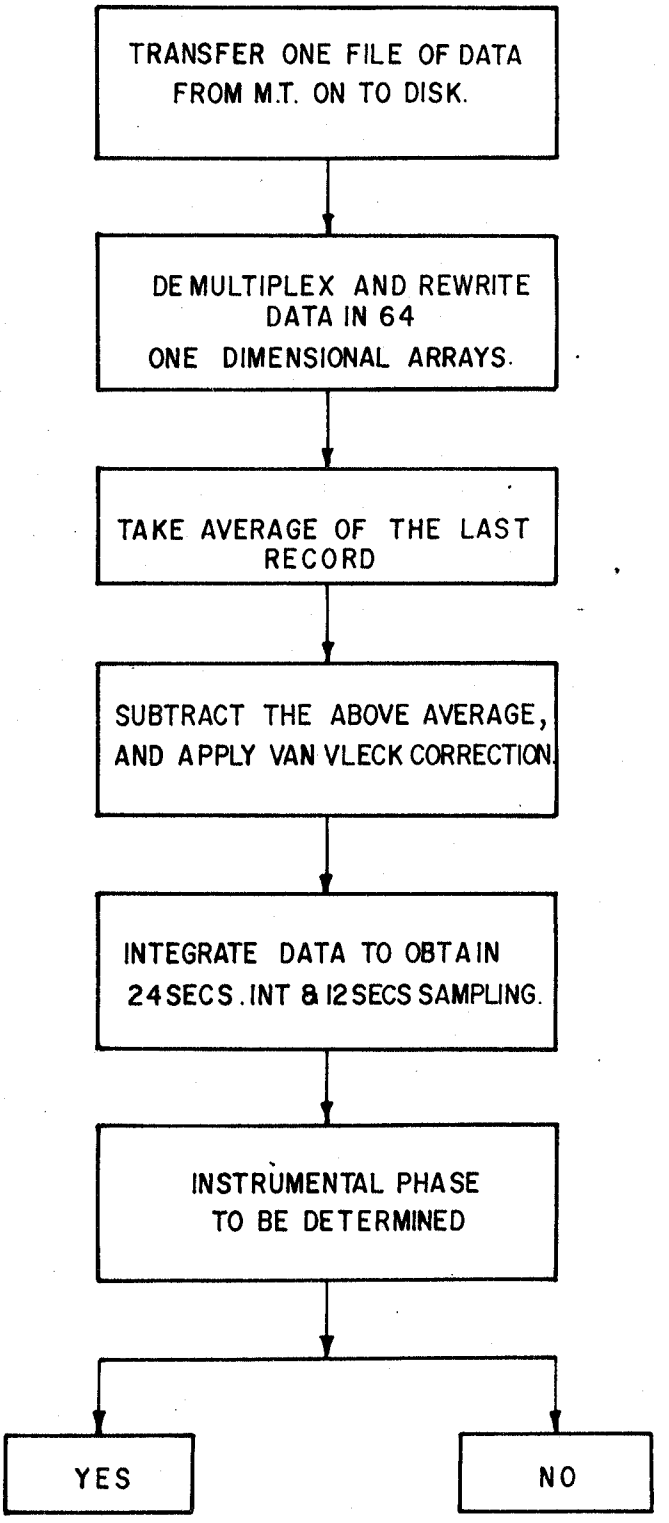

FIG. 4·7A DATA DEMULTIPLEXING.

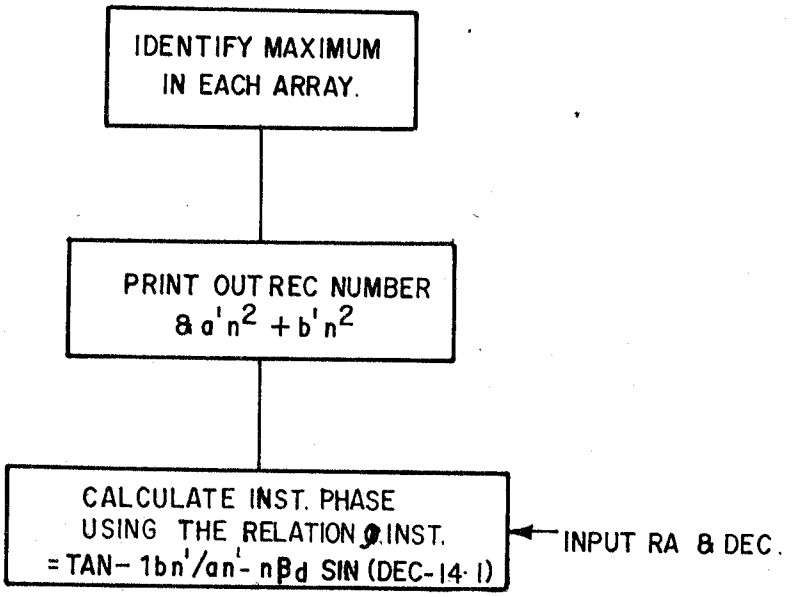

FIG. 4·7B INSTRUMENTAL PHASE DETERMINATION.

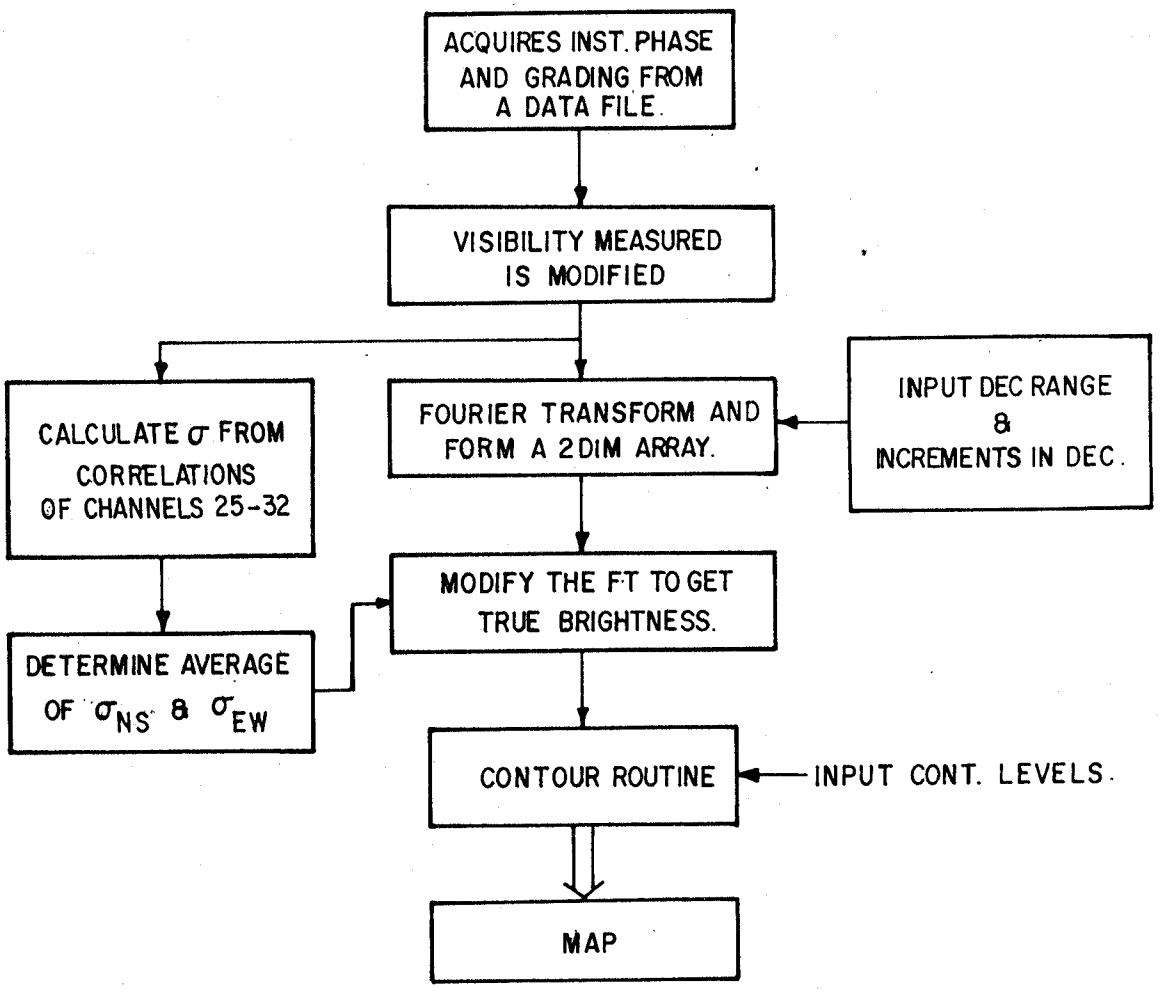

FIG. 4·7C ESTIMATION OF BRIGHTNESS DISTRIBUTION.

contains 427 records.

2. Demultiplexing

Visibilities correponding to different interferometers are recorded sequentially. They are demultiplexed and the visibilities of each interferometer are arranged in a one dimensional array.

3. Baseline Removal

For a true zero-cross detector, the correlation ρ_c of the infinitely clipped noise is related to the correlation ρ of the uncilpped noise by the Van Vleck relation

$$\rho = \sin\left[\frac{\pi}{2}\rho_c\right] \qquad (4.1)$$

If the zero-cross detector has a bias, and acts like a finite threshold detector, (V_{TH}) ρ_c and ρ are related by the equation

$$\rho = \sin\left[\frac{\pi}{2}\rho_c\right] - \beta^2/(1-\beta^2) \qquad (4.2)$$

Where $\beta = \left|\frac{V_{TH}}{\sigma}\right|$ and σ is the amplitude variance of the noise (Davis, 1974). This is a useful approximation valid only for sufficiently small values of bias V_{TH}. For $\beta = 0$ this reduces to the Van Vleck condition.

Thus for a non-ideal zero-cross detector β^2 has to be determined before ρ can be determined from ρ_c. The last record in any block contains noise calibration obtained by switching off the E-W antenna and switching on the noise diodes in the field. This forces the value of $\rho = 0$. Now if one measures ρ_c for $\rho = 0$, β^2 can be determined. Thus the average of the last record gives β^2 which has to be subtracted from the measured visibilities. Since ρ_c and β^2 are very small, subtracting before or after applying the Van Vleck correction does not make much difference. This method of removing the base line assumes that the σ of noise used for the measurement of β^2 and ρ are identical. This is strictly not true. Even though care is taken to ensure that the temperature added by the noise diode is very close to the antenna temperature due to the sky, strict equalisation is not possible since the σ of the noise varies during the measurement of ρ. The variation of σ during the measurement of ρ is greater in the E-W array. The σ of the noise of the N-S elements hardly changes in an hour due to their wide beams in both N-S and E-W directions. Thus to avoid discrepancy in the measurement of β^2, the E-W Z.C.D. is made as nearly as possible "ideal".

4.6.1 Post Integration

The E-W antenna is 1.37 kms long and gives a resolution of 21'. The sky as seen by this antenna does not change much in about 84 secs (Resolution expressed in time). Thus it is not required to have brightness points 256 msecs apart. To ensure that peaks in the brightness, distribution are sampled to atleast 98% of their value, the brightness should be sampled every 30 seconds. In the present analysis a single data point is obtained by averaging 3 records. Thus the total integration time is 24 secs. To satisfy the Nyquist criterion for sampling, a data point is produced every 12 seconds by interlaced box-car averaging.

4.6.2 Determination Of Instrumental Phase

In a two element interferometer, the cosine and sine correlator values can be directly taken as the visibility function only when the lengths of cables of the elements are exactly equal. If the cable lengths are only approximately equal and introduce a differential phase shift $\phi_{inst}(\phi_i)$, then the measured correlation coefficient have to be corrected before obtaining the brightness distribution.

Let θ be the zenith angle of a source (refer Fig.4.8). Let us consider the visibility as measured by a two element interferometer. Let the unequal lengths of cables introduce a phase ϕ_i.

True visibility = $a_n + jb_n$

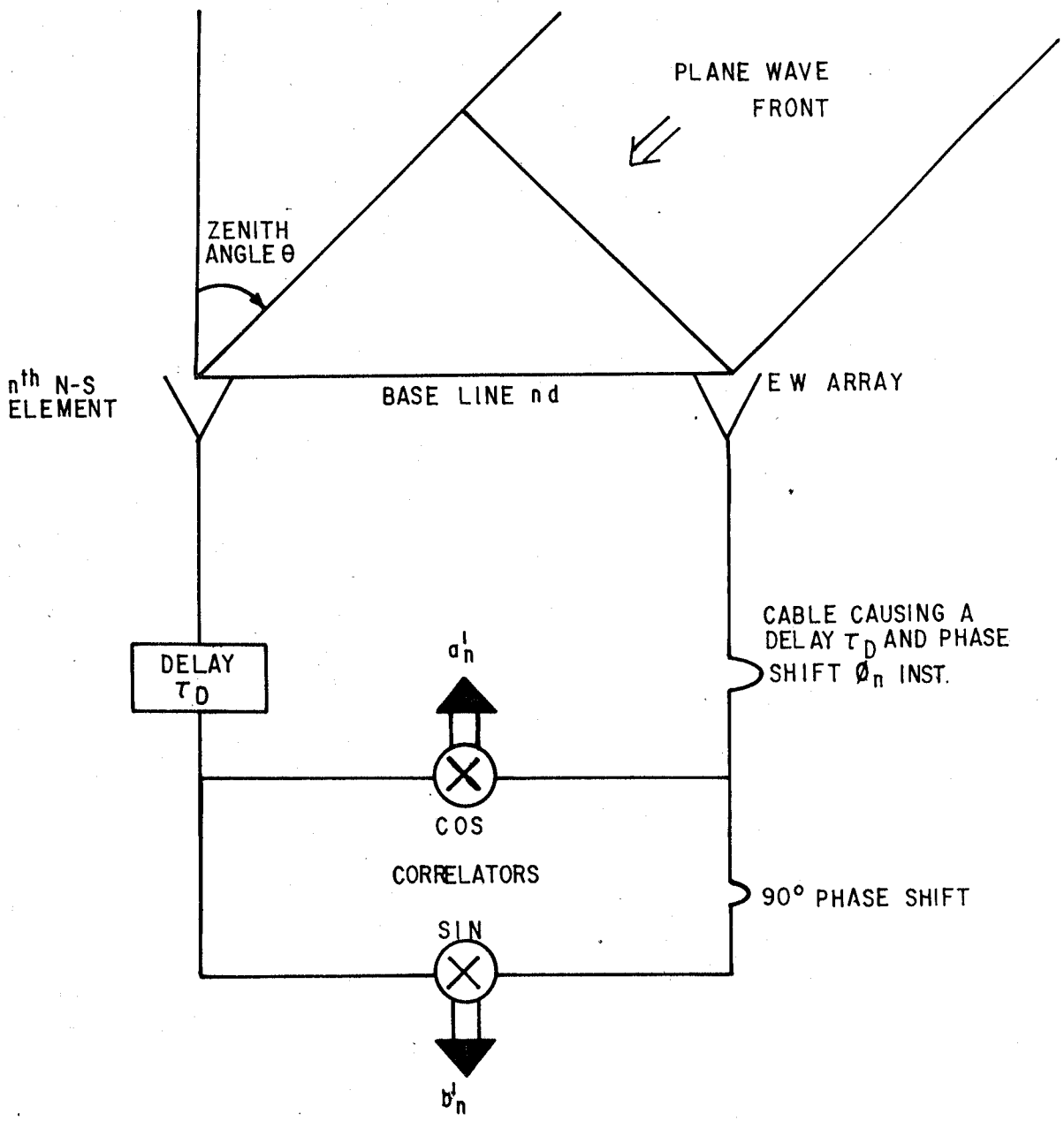

$$a'_n = \cos\left(\frac{2\pi}{\lambda} nd \sin\theta + \phi_{n\,inst}\right)$$

$$b'_n = \sin\left(\frac{2\pi}{\lambda} nd \sin\theta + \phi_{n\,inst}\right)$$

FOR A STRONG POINT SOURCE IN THE DIRECTION θ

FIG. 4·8 VISIBILITY MEASURED BY A TWO-ELEMENT INTERFEROMETER.

$$= \cos(n\beta d \sin\theta) + j \sin(n\beta d \sin\theta) \qquad (4.3)$$

$$\left[\beta = \frac{2\pi}{\lambda}\right]$$

Measured visibility

$$= a'_n + j\, b'_n$$

$$= \cos(n\beta d \sin\theta + \varphi_{ni}) + j \sin(n\beta d \sin\theta + \varphi_{ni}) \qquad (4.4)$$

where a'_n and b'_n are the cosine and sine correlation coefficients measured by the nth interferometer.

$$a_n = a'_n \cos\varphi_{ni} + b'_n \sin\varphi_{ni} \qquad (4.5)$$

$$b_n = b'_n \cos\varphi_{ni} - a'_n \sin\varphi_{ni} \qquad (4.6)$$

Thus to obtain the true visibility, one needs to measure or determine φ_{ni}. In the present case one of the elements of the interferometer is the E-W array which contains 640 dipoles and there are 23 N-S elements each with 16 dipoles. Any laboratory method to determine φ_{ni} will be too cumbersome and inaccurate. An additional complication arises since these dipoles are phased using phase shifters for observing different patches of sky. Since all the phase shifters are not identical φ_{ni} for the same interferometer will be different for different phase shifter settings. The present analysis uses a simple technique based on a priori knowledge of source positions in the sky. If a source position is known then the ratio $b_n / a_n = \tan(n*\beta*d*\sin\theta)$

is known. If $a_n' + j\,b_n'$ is the measured visibility, then $b_n'/a_n' = \tan(n*\beta*d*\sin\theta + \phi_{ni})$. Therefore, having measured a_n', b_n' and knowing Sin θ, ϕ_{ni} can be determined by using the relation

$$\phi_{ni} = \tan^{-1}(b_n'/a_n') - n\beta d \sin\theta \qquad (4.7)$$

where n = 0 to 23. The above procedure assumes that when the source is transiting, the visibility measured is only due to the point source under consideration. This is true for strong point sources and for non-zero baseline interferometers. It is difficult to find strong point sources in all zones, particularly in southern declinations. Another difficulty with this technique is, due to ionospheric refraction which is very common at decametric wavelengths, If a source is refracted by $\Delta\theta$, then

$$b_n/a_n = \tan[n\beta d \sin(\theta+\Delta\theta)] \qquad (4.8)$$

For small values of $\Delta\theta$

$$b_n/a_n = \tan[n\beta d (\sin\theta + \cos\theta \sin\Delta\theta)] \qquad (4.9)$$

Then the instrumental phase determined using a source S_1 whose position is θ, is

$$\phi_{ni}^{S_1} = \phi_{ni} + n\beta d \cos\theta \sin\Delta\theta \qquad (4.10)$$

The ambiguity due to $\Delta\theta$ can be resolved to a certain extent by determining ϕ_{ni} with one more source. If $\Delta\theta'$ is the refraction of a source S_2 at θ'

$$\phi_{ni}^{S_2} = \phi_{ni} + \eta\beta d \cos\theta' \sin\Delta\theta' \qquad (4.11)$$

$$\Delta\phi_{ni} = \phi_{ni}^{S_1} - \phi_{ni}^{S_2}$$

$$= \beta d \left[\sin\Delta\theta \cos\theta - \sin\Delta\theta' \cos\theta'\right] \qquad (4.12)$$

If $\Delta\phi_{ni}=0$ one obtains $\Delta\theta = \Delta\theta' = 0$ and without ambiguity one might have determined ϕ_{ni}. But $\Delta\phi_{ni}=0$, can also be true even if

$$\sin\Delta\theta \cos\theta = \sin\Delta\theta' \cos\theta' \qquad (4.13)$$

Thus ϕ_{ni} cannot be determined uniquely. If one plots ($\Delta\phi_{ni}$<>n) for different interferometers it should be a straight line passing through the origin. A good straightline fit indicates that the determined phases deviate from the true ones due to refraction effects only. A scatter over the straight line fit indicates random errors (due to the ionosphere, changes in cable length and capacitance due to temperature changes and drift in the receiver system).

Let us consider the effect of uncertainty in the instrumental phase determination.

Let θ be the zenith angle of the source used for determining ϕ_{ni} and $\Delta\theta$ be the error in its position. Then the corrected visibility for a point source at θ' becomes

$$\text{Cosn}(\beta d \sin\theta' - \beta d \sin\Delta\theta \cos\theta) + j \sin(\beta d \sin\theta' - \beta d \sin\Delta\theta \cos\theta)n \quad (4.14)$$

For small values of $\Delta\theta$ and $\theta \approx \theta'$, this can be rewritten as

$$\text{Cos}[n\beta d \sin(\theta' - \Delta\theta)] + j \sin[n\beta d \sin(\theta' - \Delta\theta)] \quad (4.15)$$

Thus the effect of ambiguity in the determination of the instrumental phase is to shift the point source position by $\Delta\theta$. This is true only as long as the zenith angles of the source used for the instrumental phase determination and the source mapped are very close. This was ensured for the present analysis by determining the instrumental phase for each primary beam position of the N-S interferometer. The uncertainty $\Delta\theta$ in the source positions can be corrected by comparing the final maps with an existing high frequency map.

During the present observations solar activity was at a minimum. Thus most of the instrumental phases determined are quite accurate. The graphs show (Ref Fig. 4.9) $\Delta\phi_{ni}$ of various interferometers as measured in different zones. The random instrumental fluctuations were found to be very small. The above discussion considered the amplitude of the

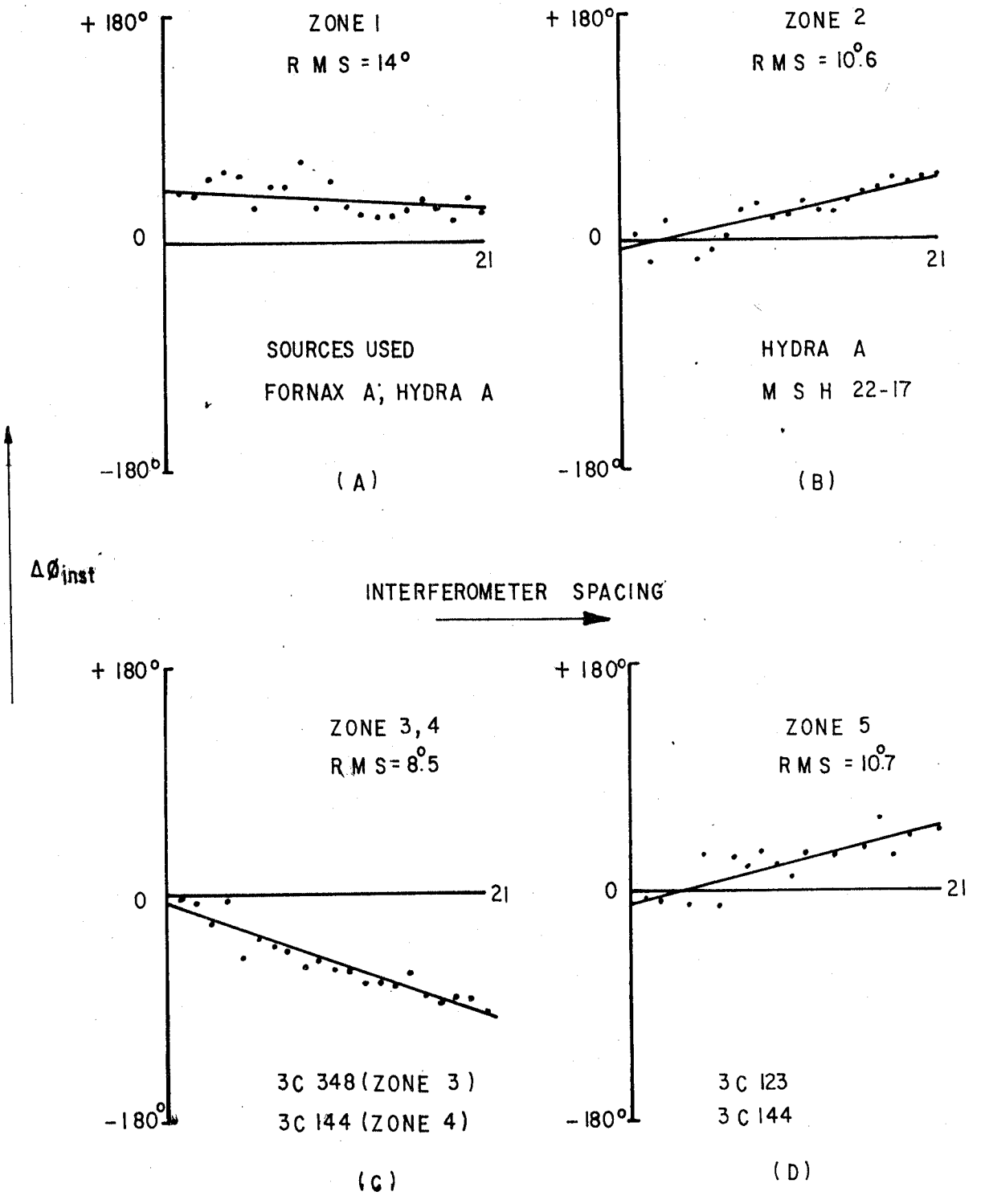

FIG. 4·9 DIFFERENCE BETWEEN INSTRUMENTAL PHASES FOR ALL INTERFEROMETERS MEASURED USING TWO POINT SOURCES WITHIN A ZONE.

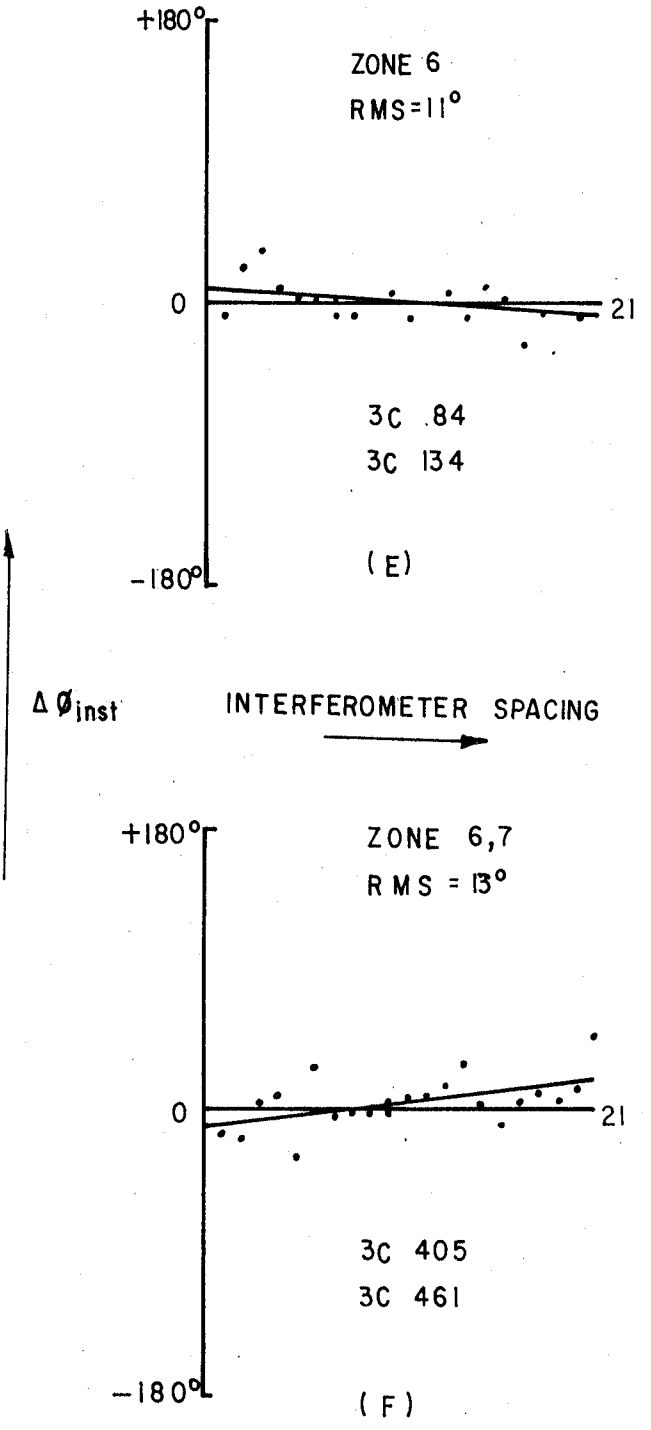

FIG. 4·9 DIFFERENCE BETWEEN INSTRUMENTAL PHASES FOR ALL INTERFEROMETERS MEASURED USING TWO POINT SOURCES WITHIN A ZONE

visibility function as unity. This has no effect on the results. But only sources which can give enough SNR in each interferometer can be used for this purpose. The software routine to determine the instrumental phase is as follows.

1. 30 minutes of data taken during the transit of a strong point source is transferred to disk.

2. The time of occurrence of maximum visibility is located in various channels.

The location of maximum is compared with the expected transit time of the source. This is done manually to ensure that interference has not occurred and that the maximum occurred at the same time in all channels.

3. The program after accepting the declination of the source (δ) and the time of transit, determines ϕ_{ni}.

4.6.3 Corrected Visibility And Grading Table

The instrumental phase is stored in a data file. Before Fourier transforming the visibility data to obtain the brightness distribution, the visibility can be graded to reduce the sidelobe levels. The grading table is also stored in a data file. The program reads the instrumental phase and grading and then corrects the measured visibility by using the following equations.

$$A_n = g_n a'_n \cos \phi_{ni} + g_n b'_n \sin \phi_{ni} \qquad (4.16)$$

$$b_n = g_n b'_n \cos\varphi_{ni} - g_n a'_n \sin\varphi_{ni} \qquad (4.17)$$

where a_n and b_n are the true visibilities, a'_n and b'_n the measured visibilities. φ_{ni} = instrumental phase and g_n = grading of the nth interferometer.

The sidelobe levels can also be suppressed after Fourier Transformation by convolving the map with the F.T. of the desired grading.

4.6.4 The Fourier Transform

The visibility and the brightness distribution are related by the equation

$$V(u) = \int_{-\pi/2}^{\pi/2} g(\theta) \cdot B(\theta) \cdot e^{\frac{2\pi}{\lambda} \cdot u \sin\theta} \cdot d\theta \qquad (4.18)$$

V(u) = visibility for an interferometer of spacing u .

$g(\theta)$ = Antenna gain as a function of θ.

$B(\theta)$ = brightness distribution in the sky.

λ = Wavelength of observation.

The above equation can be rewritten in the form

$$V(u) = \int_{-\pi/2}^{\pi/2} (g(\theta)/\cos\theta) \cdot B(\theta) \cdot e^{\frac{2\pi}{\lambda} \cdot u \sin\theta} d(\sin\theta) \qquad (4.19)$$

Thus V(u) and $[g(\theta)/\cos\theta] * B(\theta)$ form a fourier transform pair where u and sin θ are the independent variables. In other words, the fourier transform of V(u) gives the modified brightness distribution

$$M(\theta) = (g(\theta)/\cos\theta) \cdot B(\theta) \qquad (4.20)$$

The visibility function is the F.T. of the brightness which is always real. Hence the visibility function is Hermitian symmetric. Thus

$$V(-u) = V^{*}(u) \tag{4.21}$$

where * denotes the complex conjugate.

Let V(u) = a(u) + j b(u). Then it can be shown by substituting 4.21 in 4.19

$$M(\theta) = 2\int_{0}^{\infty} a(u)\,\mathrm{Cos}\left[\tfrac{2\pi}{\lambda}\cdot u \sin\theta\right] + b(u)\,\mathrm{Sin}\left[\tfrac{2\pi}{\lambda}\cdot u \sin\theta\right] \tag{4.22}$$

Since the visibility is measured at intervals of 20 metres with 23 interferometers, an estimate of M(θ) can be obtained by the Fourier Series.

$$M_e(\theta) = a_0 + 2\sum_{n=1}^{22} a_n \mathrm{Cos}\left(\tfrac{2\pi}{\lambda}\cdot nd\sin\theta\right) + b_n \mathrm{Sin}\left(\tfrac{2\pi}{\lambda}\cdot nd\sin\theta\right) \tag{4.23}$$

where u = n*d ;n = 0 to 22

d=20 m ; λ = 8.695 m

The present program accepts the declination range and increments of θ for the calculation of $M_e(\theta)$ by using the corrected visibilities.

4.6.5 Total Power Measurement

The visibilities are obtained using a one-bit correlator. If ρ_{12} and R_{12} are the visibilities measured in a one-bit and an analog correlator,

$$\rho_{12} = R_{12} / \sigma_1 \sigma_2 \qquad (4.24)$$

where σ_1 , σ_2 are the R.M.S. noise fluctuations of the input signals. If one uses ρ_{12} for the F.T., then $M_e(\theta)$ has to be modified by multiplying it by σ_1 , σ_2 . The method of determining σ_1 and σ_2 using a one-bit correlator is described in section 2.7. The program uses an analytical expansion for the error function and calculates σ by knowing V_{TH} in channels 25-32 by the method of bisection. Four threshold detectors are used to measure σ . Their average value is used for analysis.

4.6.6 True Brightness From Modified Brightness

The true brightness $B(\theta)$ at any given time is given by

$$B(\theta) = M_e(\theta) \cdot \sigma_{EW} \cdot \sigma_{NS} \cdot \frac{\cos\theta}{g(\theta)} \qquad (4.25)$$

$M_e(\theta)$ = obtained by the fourier series

σ_{EW} , σ_{NS} = R.M.S. fluctuations of the inputs at any given time

$\cos\theta$ = cosine of the angle at which brightness is required.

$g(\theta)$ = Antenna gain as a function of θ , where

$$g(\theta) = P(\theta) \cdot f(\theta) \qquad (4.26)$$

$P(\theta)$ = normalised power pattern obtained by multiplying the voltage pattern of the E-W array in the N-S direction and the average voltage pattern of the N-S interferometer

elements.

$f(\theta)$ = variation of the gain of the array with zenith angle.

If $f_{EW}(\theta)$ and $f_{NS}(\theta)$ are the gain variations of E-W and N-S array with zenith angle θ

$$f(\theta) = \sqrt{f_{EW}(\theta)\ f_{NS}(\theta)} \qquad (4.27)$$

$f_{EW}(\theta)$ and $f_{NS}(\theta)$ are calculated by using the theorems of reciprocity and power . The reciprocity theorem states that the antenna characteristics are identical whether transmitting or receiving. The power theorem states that the total power radiated is given by the integral of the radiation intensity over a solid angle of $4*\pi$.

$$W = \int_{4\pi}\int [\text{Radiation. int}]\, d\Omega . \qquad (4.28)$$

If $P_n(\theta\varphi)$ is the normalised power pattern and g is the gain of the antenna

$$g = P(\theta,\varphi)_{.max.} \qquad (4.29)$$

$$W = g \int_{4\pi}\int P_n(\theta,\varphi)\, d\Omega \qquad (4.30)$$

This integral is called as the beam solid angle. For a transmitting antenna the total power radiated from it is independent of the phasing of the array. Thus if $P_1(\theta,\varphi)$ and $P_2(\theta,\varphi)$ are the normalised power patterns when phased in different directions, the gains g_1 and g_2 obey the condition that

$$g_1 \iint_{A\pi} P_1(\theta,\varphi)\, d\Omega = g_2 \iint_{4\pi} P_2(\theta,\varphi)\, d\Omega \qquad (4.31)$$

$f_{EW}(\theta)$ and $f_{NS}(\theta)$ were obtained by using the above equation. Their gains when phased to the zenith were taken as unity. The direction cosines were used for simplicity.

Note: Only a planar array with a beam narrow in both directions, and which does not have grating lobes, behaves like a continuous sheet. It's gain varies as Cos θ which is similar to Lamberts cosine law in optics. A linear array behaves similar to the planar array only in the broadening of its beamwidth when phased in directions away from the zenith. For both the arrays, the beamwidth in the plane of scan varies approximately inversly as Cos θ. But the gain of a linear antenna does not decrease in a similar fashion. When a linear array is scanned in the θ direction, its beam broadens by Sec θ in that direction but the extent of the beam decreases by a factor Sec θ in the perpendicular direction. Thus the beam solid angle, and hence the gain, remain constant. When a planar array is scanned, broadening takes place only in the direction of scan. In the perpendicular direction, where the beam is narrow, the beam does not get limited in its extent by the sky. Thus the beam solid angle increases by approximately sec θ decreasing the gain by the same factor. Instead of using pattern integration, the gain of an array can also be determined if self and mutual impedances are known.

The graphs show (Fig. 4.10) the gain variations of the E-W and N-S arrays with zenith angle. The departure from cos θ is negligible upto 30° zenith angles. For zenith angle >30° the departure is noticeable. For θ> 48° grating lobes appear and the departure is significant.

The program calculates the true brightness from $M_e(\theta)$ by using the equation

$$B(\theta) = \frac{M_e(\theta)}{P(\theta)} \cdot \sigma_{EW} \cdot \sigma_{NS} \cdot \frac{\cos\theta}{\sqrt{f_{EW}(\theta)\, f_{NS}(\theta)}} \qquad (4.32)$$

4.7 CALIBRATION OF THE MAP

Contour levels in a map can be calibrated by knowing the flux densities of a few point sources in the regions synthesized. These sources called calibrators should possess the following qualities.

1. They should have small angular sizes compared to the beam size. If the sources have angular dimensions large enough to be resolved, then corrections for finite angular size becomes necessary. This causes calibration errors.

2. They should not be variables.

3. They should have a simple, preferably linear, spectrum.

4. The fluxes of the calbirators should not be too high to avoid non-linearity problems, in the receiver system.

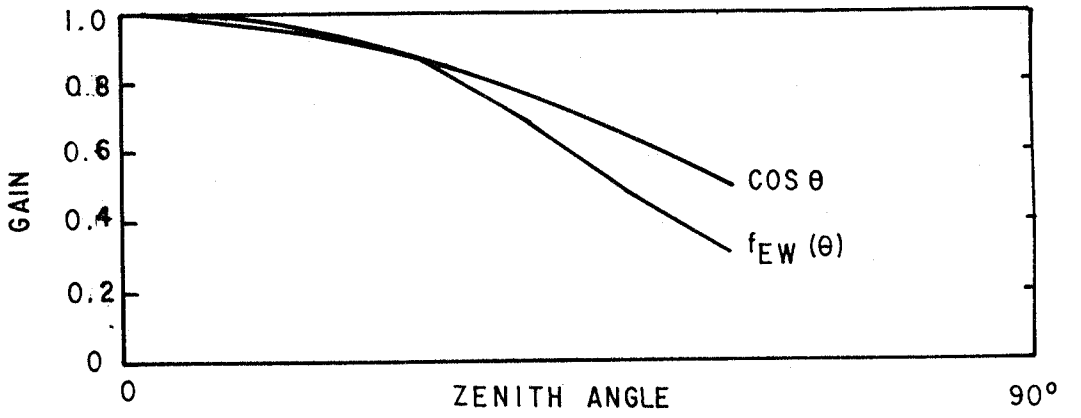

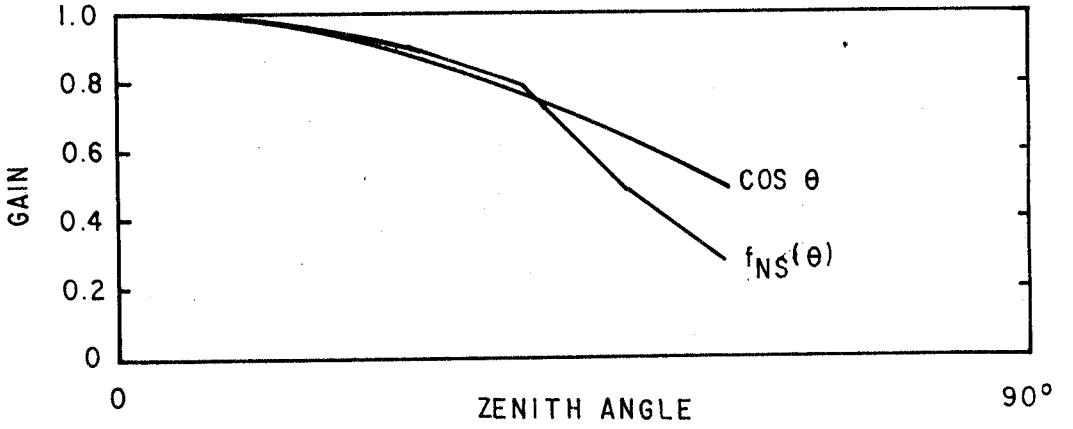

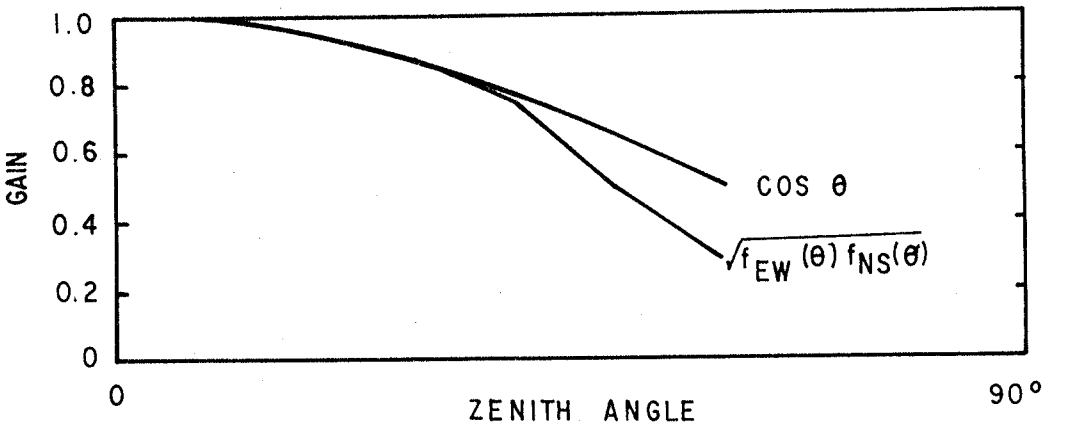

FIG. 4·10 GAIN VARIATIONS OF E-W AND N-S ARRAYS.

Having selected suitable sources their absolute flux densities can be measured. This requires careful calibration of both the receiver and the antenna. For large antennas like the one at Gauribidanur, computation of the absolute gain of the antenna cannot be done satisfactorily because of the difficulties in accounting for the effects of ground reflections, losses and mutual impedances. Direct measurement by conventional methods is also not feasible for the Gauribidanur antenna on account of the large number of dipoles and preamplifiers. A.G. Little (1958) has suggested a technique of calibrating such large aerials in terms of a smaller one whose gain can be accurately calculated. This requires setting up a standard dipole. Such an absolute measurement is beyond the scope of the present work. Another method of obtaining the fluxes of calibrators at the required frequency is to use the spectral index data and fluxes measured at other frequencies. The present work used the 38 to 750 MHz spectral indices and the 38 MHz fluxes of the calibrators as given by Kellermann, et.al. (1969), in their revised 3C catalogue. This is one of the most detailed surveys at frequencies very close to 34.5 MHz. They used absolute flux density measurements of a number of strong sources made by Williams, et.al. (1966), for their survey. The table shows the ratio of the flux computed at 34.5 MHz to the deflection (F/d) obtained in our instrument. The deflection (d) was obtained from the E-W and N-S patterns of the calibrators. If d_1 is the peak deflection of the beam and d_2 and d_3 are the first sidelobe

level deflections,

$$\text{deflection} = \frac{1}{1\cdot 2}\left[d_1 - \frac{d_2 + d_3}{2} \right] \qquad (4.33)$$

A sinc function fitting for the beam will give better results. This approach of measuring the deflection was used because of its simplicity. Sources which are listed as telescope calibrators by K.P.W. and Baars et.al. (1977), were chosen for calibrating the deflection. A sufficient number of sources were chosen to cover the right ascension declination and flux ranges of the maps presented (refer Fig. 4.11). The RMS variation of F/d is found to be 15% for the calibrators whose N-S and E-W patterns did not deviate much from the theoretical beam shape (sinc function). The accuracy of the flux determination at 38 MHz quoted by K.P.W. is around 5 to 15% (Table 4.2). Thus, the R.M.S. fluctuation of the flux / deflection is quite satisfactory. Further, the ratio of flux to deflection of the sources shows no dependence on declination, R.A., Spectral index or the flux of the calibrators themselves. These are shown in figure 4.12.

With the general improvement of accuracy in the flux density measurements, in the past few years, many researchers have investigated the flux density scales for radio sources at different frequencies. Braude, et.al. (1970), who have made one of the most detailed investigations at low frequencies, suggest that the K.P.W. scale for the stronger sources is low by 9% at 38 MHz while

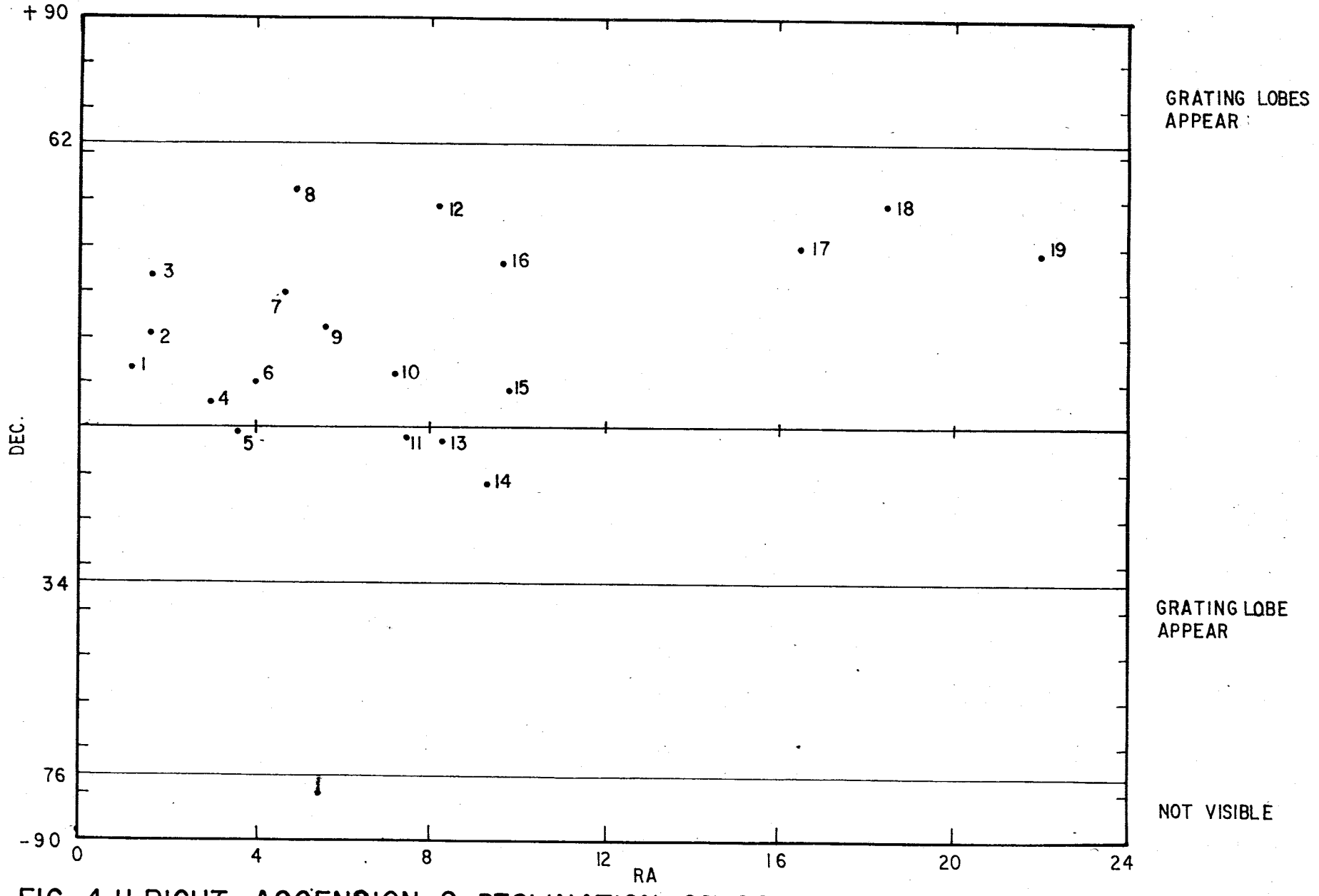

FIG. 4.11 RIGHT ASCENSION & DECLINATION OF SOURCES USED FOR TELESCOPE CALIBRATION

source name	errors in the flux densities (KPW)	Flux (Jansky)	Flux / Def	Average
3C 33	a	146	6.96	
47	b	130	6.09	
48	b	66	8.19	
75	b	90	6.18	
89	b	107	8.40	
98	a	158	6.21	7.75±1.13
123	a	616	8.40	
130	b	54	7.59	
144	a	2501	9.30	
175	b	90	8.10	
180	c	55	8.43	
196	a	177	7.47	
196.1	b	103	7.83	
218	-	1242	8.67	
223	b	48	6.27	
227	a	130	7.92	
338	a	244	9.18	
380	a	226	9.69	
438	d	149	6.42	

Symbols

(a) $\sigma < 5\%$ (b) $5\% < \sigma < 15\%$

(c) $15\% < \sigma < 25\%$ (d) $25\% < \sigma < 35\%$

Table 4.2 FLUX/DEFLECTION OF TELESCOPE CALIBRATORS

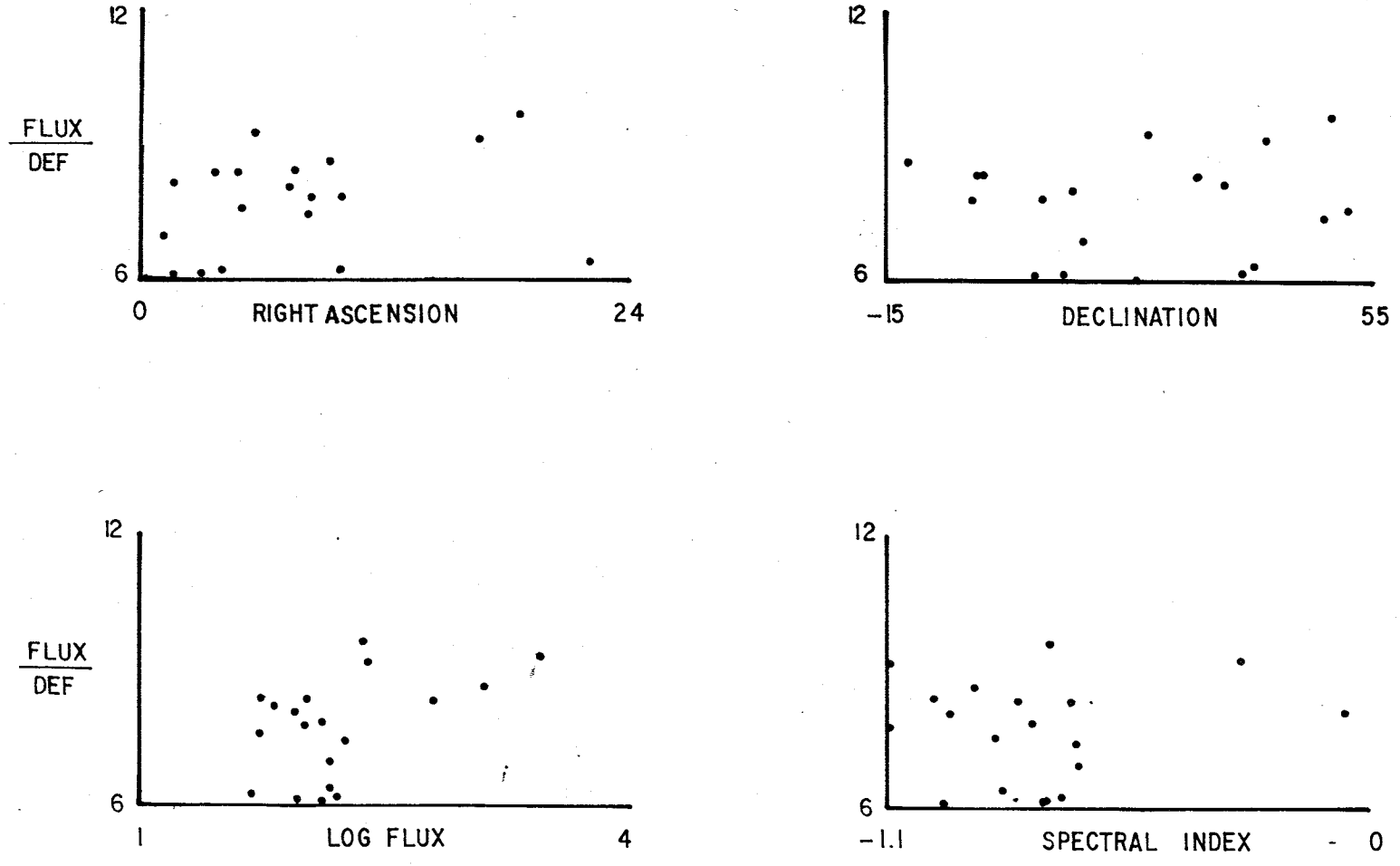

FIG. 4.12 CORRELATION BETWEEN FLUX/DEFLECTION OF TELESCOPE CALIBRATORS USED & THEIR COORDINATES, FLUX & SPECTRAL INDICES.

for the weaker sources it is low by 39%. Such a discrepancy with the K.P.W. scale has not been noticed in the present observations.

4.8 CONTINUUM MAPS

Since the early days of radio astronomy, several attempts have been made to prepare maps of the radio continuum brightness of the whole sky. Droge and Priester published the first all sky map at 200 MHz. Yates in 1968 and Landecker in 1970 prepared all sky maps at 85 and 150 MHz. Cane in 1978 published an all sky survey at 30 MHz. These maps were produced by combining data not all of which were obtained at the same frequency. Haslam et.al. published an all sky survey in 1981 by using the data collected through a series of observations at 408 MHz. Their atlas offers considerable improvement in resolution over previous all sky maps, and also an improved level of consistency in resolution and calibration. An all-sky survey similar to the one made at 408 MHz, does not exist near the operating frequency of our telescope. Our telescope, because of its geographical location, can cover the declination range of -76° to $+90^{\circ}$, and a large portion of this range can in principle be mapped by the present receiver system. Maps available close to our operating frequency are listed below.

1. Contour maps of brightness temperature at 38 MHz for the range of declination $+15^{\circ} < \delta < +90^{\circ}$, prepared by P.J.S. Williams, S. Kenderdine and J.E. Baldwin in 1966 with a resolution of approximately 45'. They had a sensitivity of 15 Jy.

2. A survey of the region of sky between declinations -4° and -64° at a frequency of 30 MHz with a resolution of $0^{\circ}.8$ at zenith as published by Bevan Jones (1973).

3. Milogradov-Turin and F.G. Smith published a 38 MHz survey, with a beamwidth of $7^{\circ}.5$ covering the declination range from -25° to $+70^{\circ}$. This map was intended for comparison of spectral indices of various large scale galactic features.

While the third one is a survey with a very coarse resolution, the first two were made with moveable arrays and by compiling data over a large number of days. In these surveys, lower order Fourier components were not obtained by direct observation. The present receiver system has made the Gauribidanur antenna capable of making large scale maps at 34.5 MHz with the following features.

The antenna does not use any moveable elements, and 23 visibilities can be measured simultaneously. This makes the maps more reliable than maps made with moveable elements, because at low frequencies where ionospheric refraction causes time varying shifts in the position and intensity of the sources. All the fourier components up to the zeroth

order can be obtained by direct observation. This helps to observe large scale features in the galaxy. With the rearrangement of the E-W array, the entire range in declination can be mapped in a time of the order of one day. While such a large scale survey is beyond the scope of the present work, only a few maps are presented here to establish the suitability of the instrument for such a large scale survey.

The maps are presented in Equatorial Coordinates. Because of the gradual precession of the earth's axis, the equatorial coordinates for a fixed object in the sky change with time. Hence, it is necessary to specify the epoch which the R.A and declination of the sources refer to. Maps were initially prepared in 1984.5 coordinates and were later transformed to epoch 1950. As this transformation distorts the rectangular grid, the maps presented here use the best fit rectangular grid for 1950 coordinates. This resulted in positional inaccuracies of approximately 5 secs of time in Right Ascension and $3'$ in declination. Galactic longitude and latitude lines are also shown on the maps. The number of contours labelled depend on their density. The brightness temperature corresponding to the contours can be obtained from the contour key given in the table 4.3. This table also gives the antenna and the receiver parameters. Some of the radio sources seen in these maps are described below

Antenna Parameters

Half Power width of the cosine pencil beam	=	$26' \times 41' \sec(\delta - 14^{\circ}.1)$
Beam Solid angle	=	9.02×10^{-5} Steradians
System Sensitivity	~	1 Jansky
Minimum detectable flux (confusion limited; obtained by measuring SNR with which weak sources are observed)	~	20 Jansky

Map Parameters

Countour Numbers	Deflection
1 to 6	-48 + 8(n-1)
7 to 19	2(n-7)
20 to 28	28 + 4(n-20)
29 and above	68 + 8(n-29)

Flux in Jys = 7.75 deflection

Brightness Temperature = $[308 \times 7.75/\sec(\delta - 14^{\circ}.1)]$ deflection

Table 4.3

MAP- 1

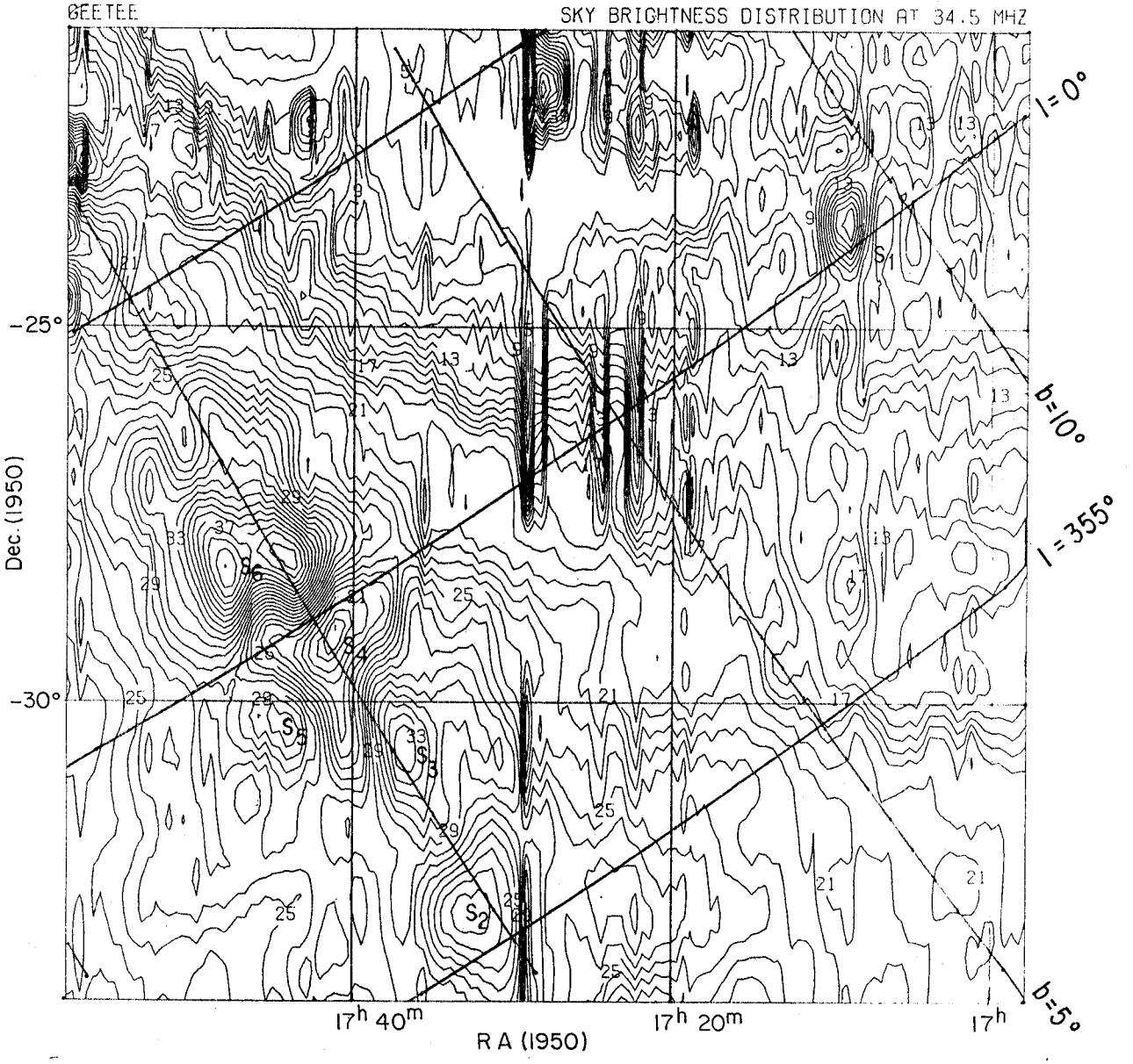

S_1 = MSH 17-23, S_3 = MSH 17-39, S_2, S_4 = ABSORPTION REGIONS,

S_5, S_6 = EMISSION REGIONS

MAP-2

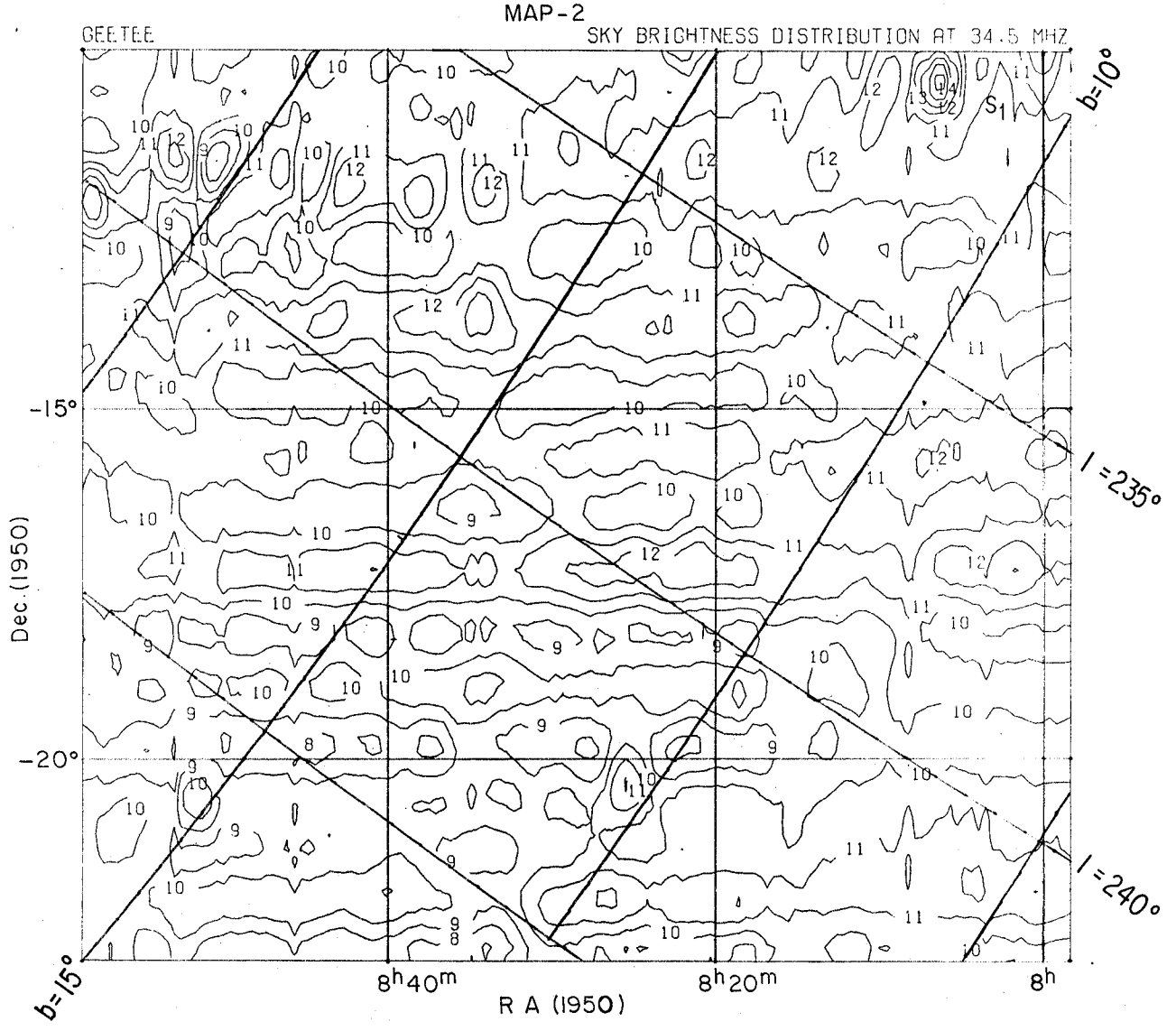

S_1 = Observed at 408 MHz by Haslam et. al. (1981)

MAP-3

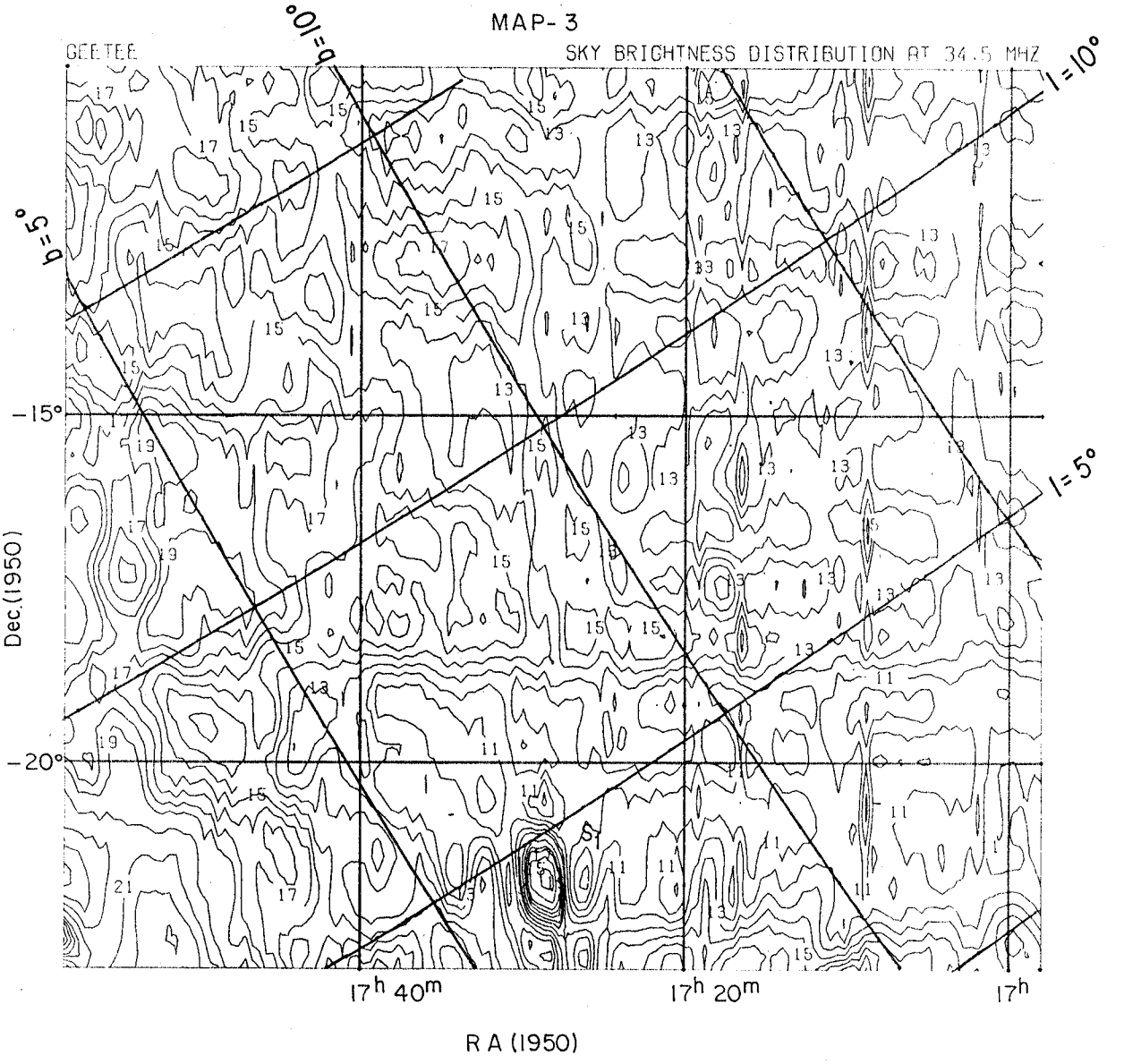

S_1 = KEPLER'S SUPERNOVA REMNANT.

MAP- 4

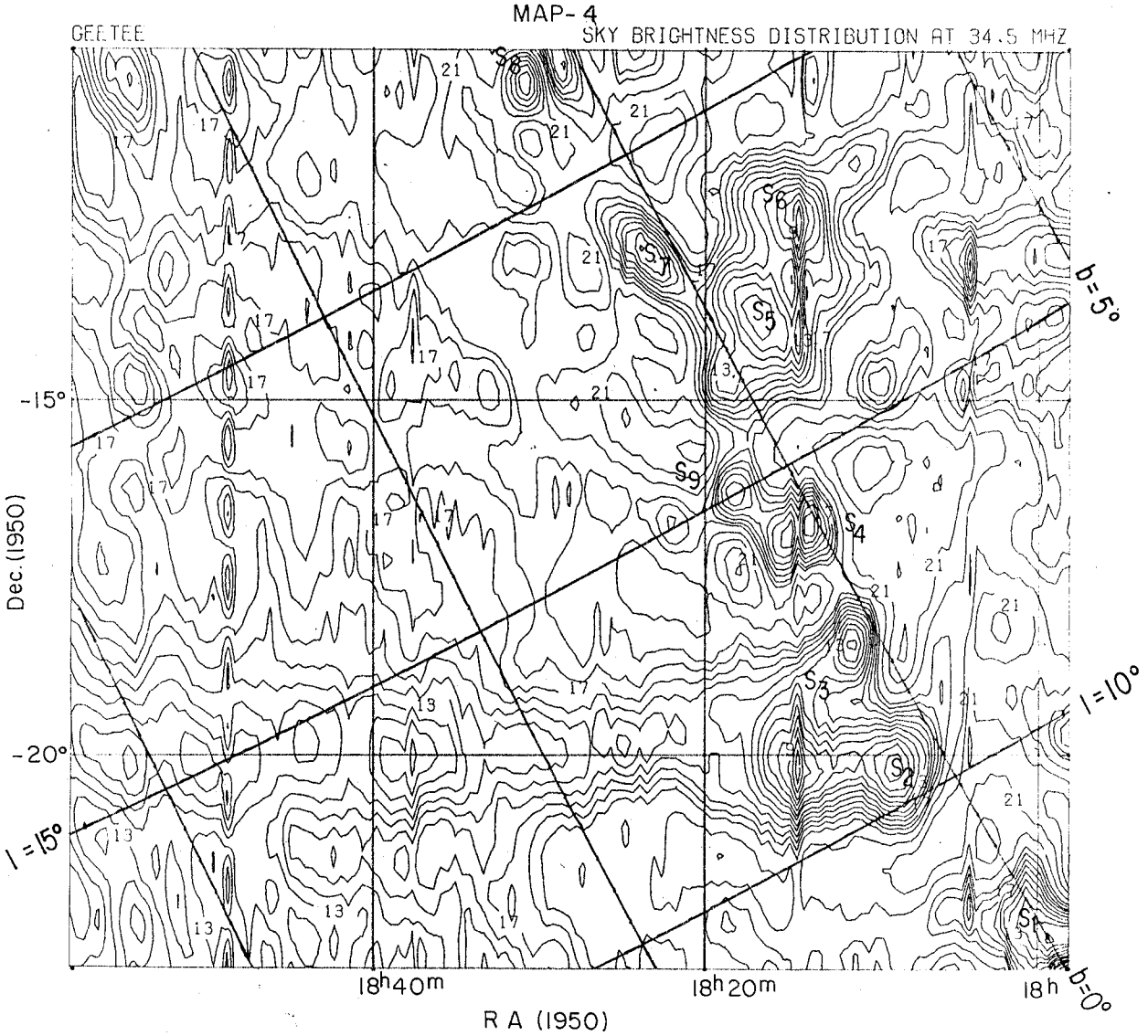

S_1 = CTB 47, S_2 = CTB 49, S_3 = MSH 18-13, S_4 = MSH 18-14, S_5 = CTB 51(M16), S_6 = CTB 60, S_7 = CTB 53, S_8 = MSH 18-113, S_9 = CTB 52 (M17).

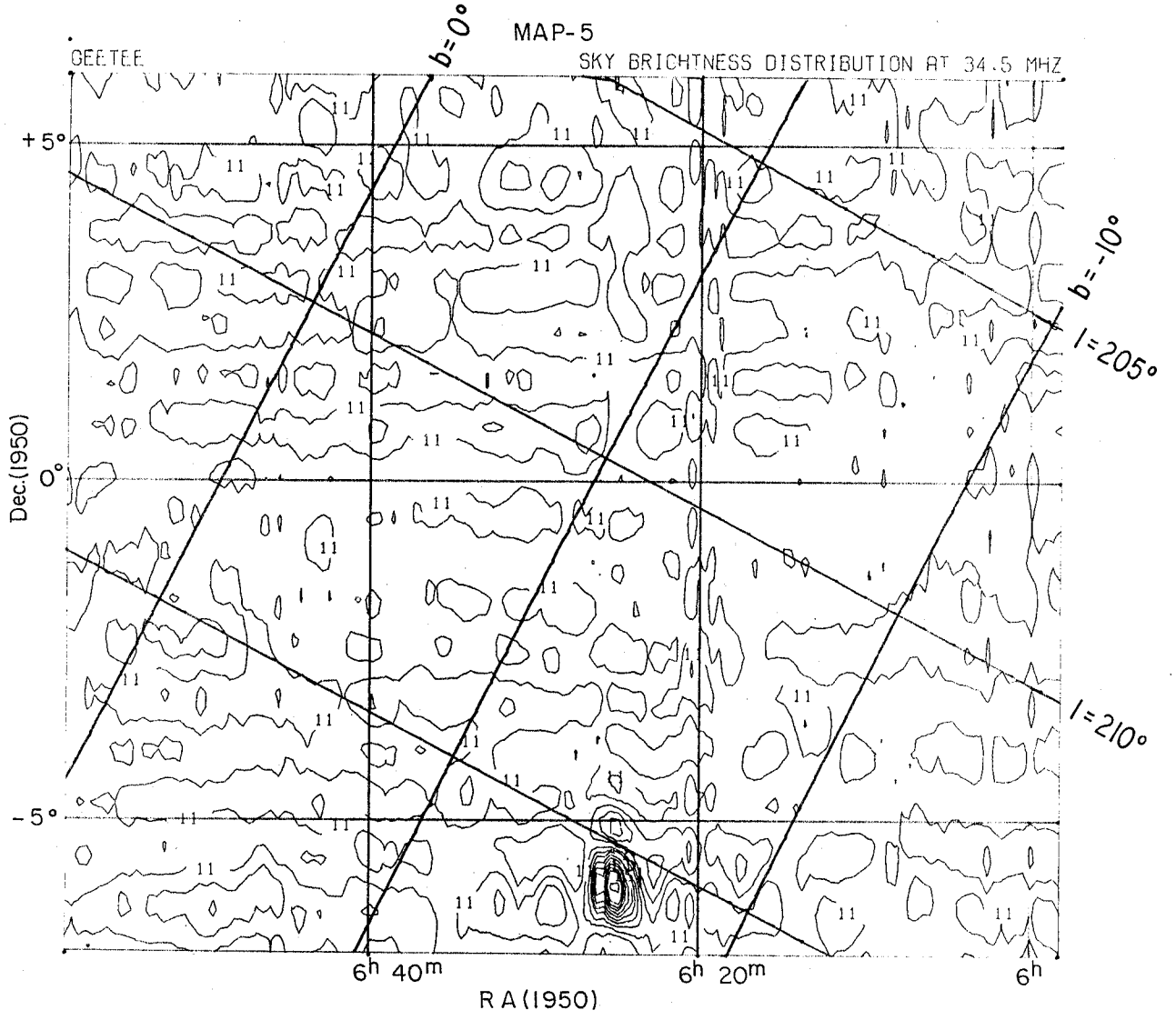
MAP-5
GEETEE
SKY BRIGHTNESS DISTRIBUTION AT 34.5 MHZ
b=0°
b=-10°
l=205°
l=210°
+5°
0°
-5°
Dec.(1950)
6h 40m
6h 20m
6h
RA(1950)

S_1 = CTA 42

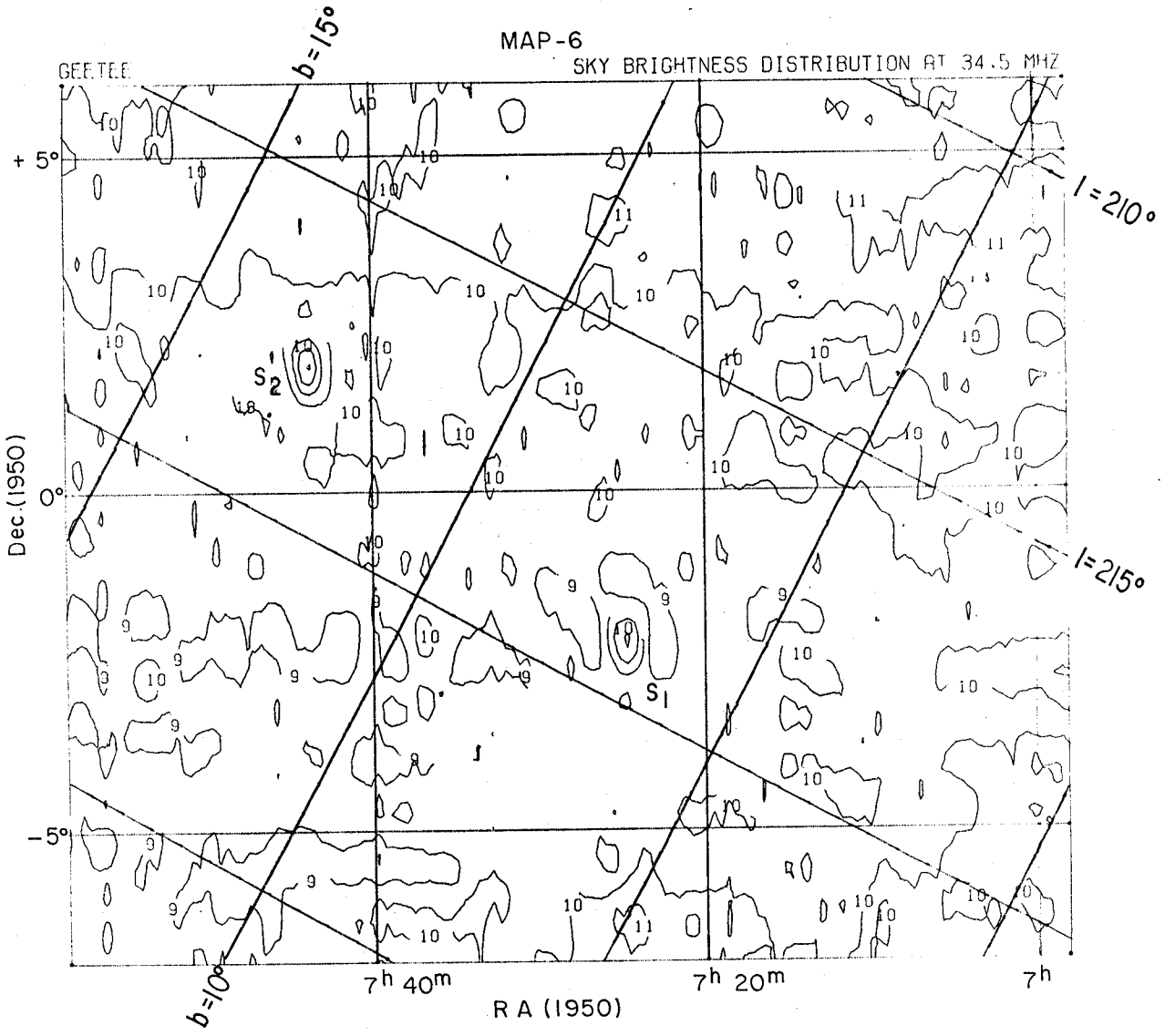

S_1 = 3C180, S_2 = 3C187

MAP-7

SKY BRIGHTNESS DISTRIBUTION AT 34.5 MHZ.

GEETEE

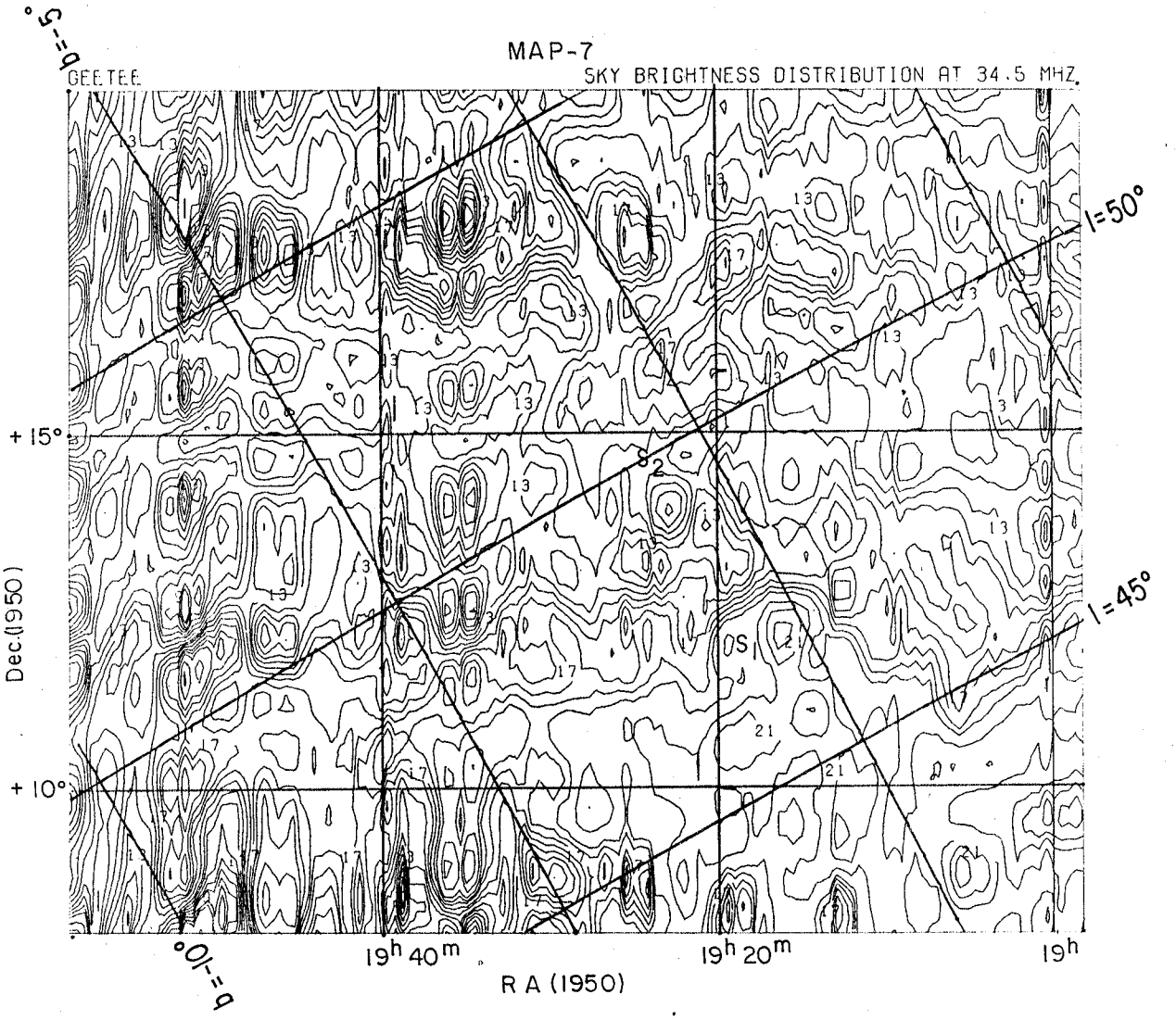

S_1 = HC 30 , S_2 = W51

MAP - 8

GEETEE SKY BRIGHTNESS DISTRIBUTION AT 34.5 MHZ

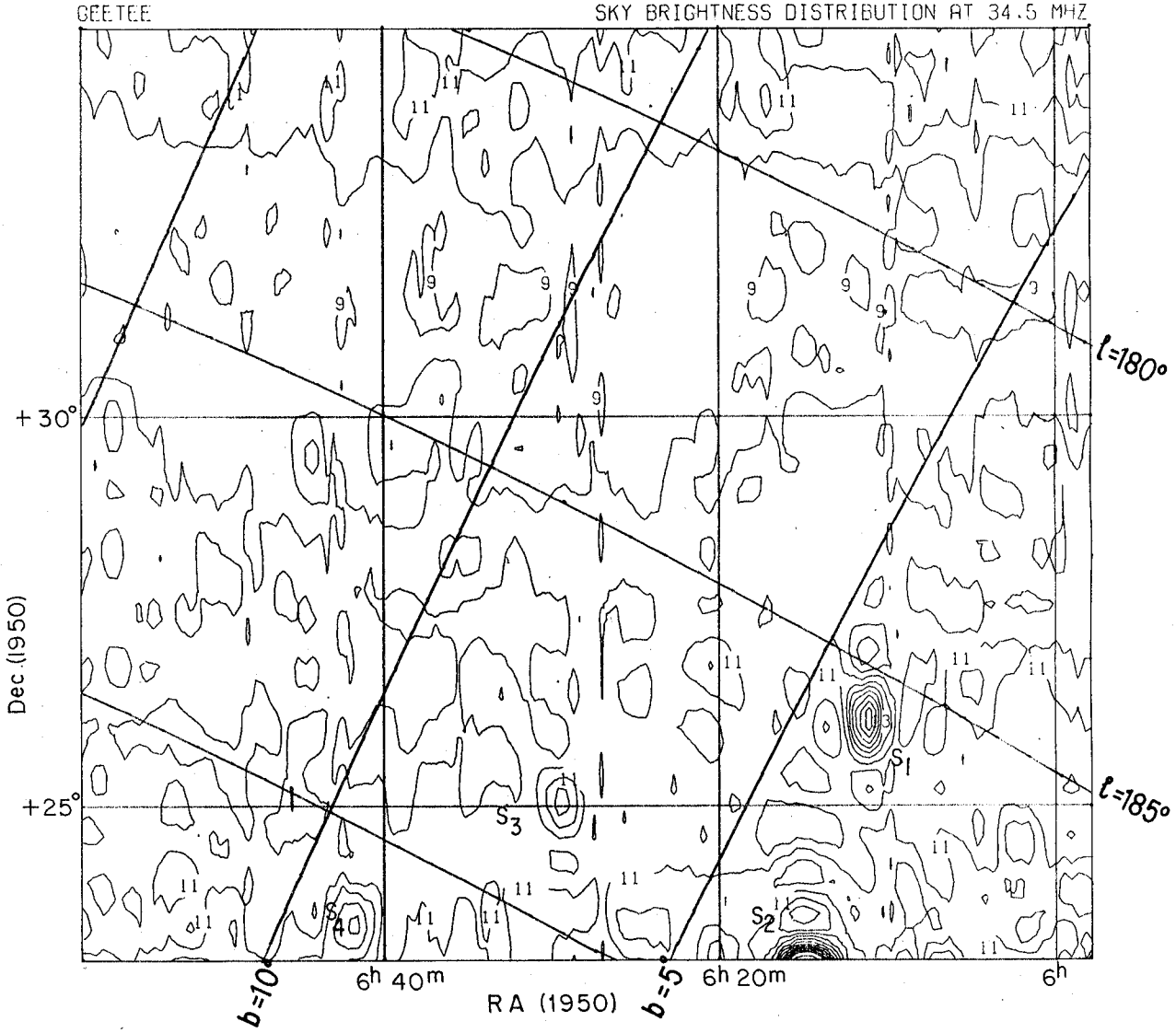

S_1 = 3C154 S_2 = IC 443 S_3 = 4C 25.18 S_4 = 3C165

MAP-9

GEETEE

SKY BRIGHTNESS DISTRIBUTION AT 34.5 MHZ

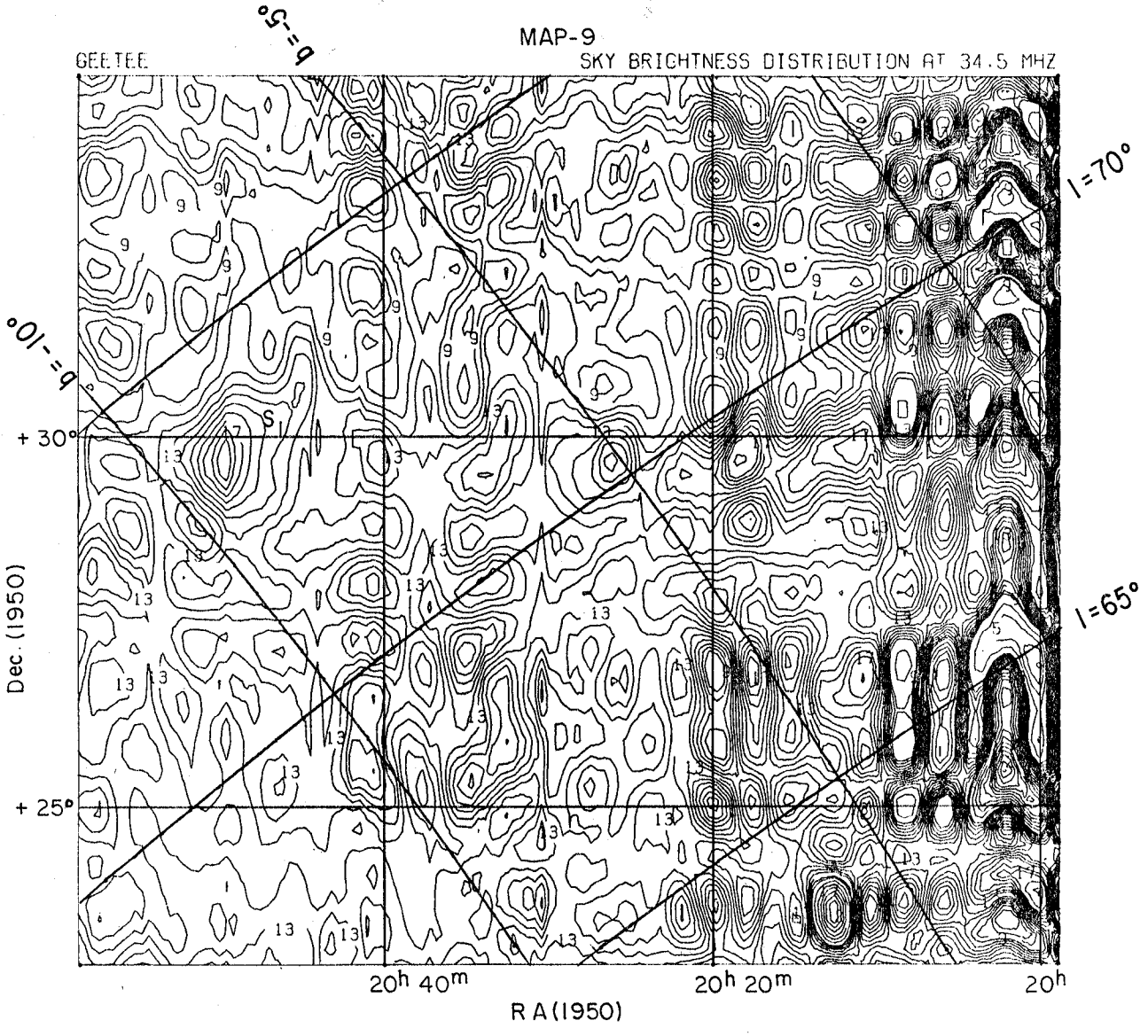

S_1 = CYGNUS LOOP

MAP-10

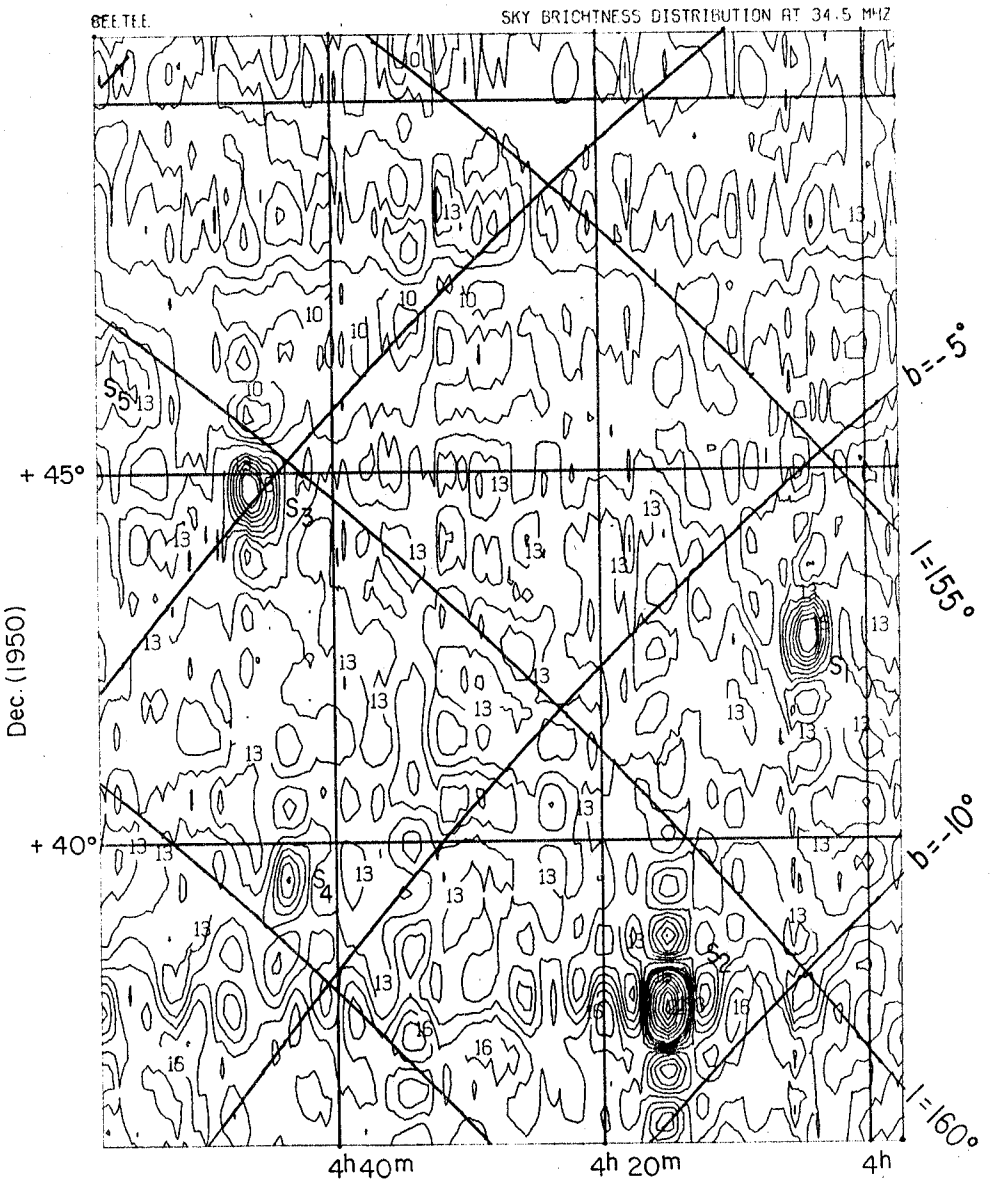

S_1=3C 103, S_2=3C 111, S_3=3C 129, S_4=3C 125, S_5=HB 9

4.8.1 Supernova Remnants

A supernova explosion is the end of the stellar evolution for certain types of stars. In a comparatively short time, the outer shell of the star is expelled with a large amount of kinetic energy. The expanding envelope and its interaction with the surrounding medium is the supernova remnant. A supernova remnant manifests itself in the X-ray, Optical and radio regions of the spectrum. The evolution at each wavelength has its own characteristics. The radio emission is an important characteristic feature of the supernova remnants. The identification of a galactic source as a supernova remnant is generally made on the basis of the non-thermal nature of its radio spectrum (M. Duin, 1974)

Cygnus Loop (Map 9): The Cygnus loop is probably one of the oldest supernova remnants observed. It has been studied extensively in the range 200 MHz and above with high resolution. Low frequency observations of this loop will help to study the variations in the radio structure of the nebula and the spectral index of the different parts of the loop. Other observations of the Cygnus Loop at low frequencies are due to Sastry et.al. (1981) and Abranin et.al. (1977).

Kepler (Map 3): This is a supernova remnant whose outburst was observed by Kepler in 1604 A.D.

HB9 (Map 10): This source was first observed by Hazard and Hanbury Brown during a general survey of the galaxy. HB9 is located in the constellation Auriga. William et.al. (1966). K.S. Dwarakanath et. al. (1982) have also obtained maps of this remnant at 38 MHz and 34.5 MHz respectively.

4.8.2 Galactic Plane And HII Regions

In the study of the galactic continuum emission,it is very important to understand

a) its attenuation at low radio frequencies and

b) the contribution of non-thermal sources to it.

The Milky Way is thought to be a spiral galaxy with a diameter of about 30 kpc. The galaxy is conveniently separated into three components namely Disk, Nucleus and Halo. The radio galactic background is due to both synchrotron and thermal radiations. The appearance of the galaxy is different at high and low radio frequencies due to the different radio spectra of these two mechanisms. At high frequencies most of the radiation from the galaxy is of thermal origin. 5 to 10% of the mass of our galaxy is in the form of interstellar ionized hydrogen. In the absence of any exciting sources, the hydrogen remains in its neutral state. But when a hot stellar source is in or near such a cloud, its ultraviolet radiation ionizes the cloud causing it to emit continuum radiation, characteristic of a thermal

source. These ionized hydrogen regions occur mainly within several degrees of the plane of the galaxy. At decametric wavelengths, HII regions near the galactic plane have electron temperatures lower than the brigthness temperature of the background non-thermal radiation. This results in HII regions appearing in absorption at these low frequencies. The plane of the galaxy tends to be characterised by absorptions due to such regions. Map 4 depicts several HII regions seen in absorption. Two well known ones are:

M16: This is a gaseous emission nebula. This is also believed to contain dust clouds which after a slow gradual contraction will become proto stars.

M17: This is known as the Omega or Horse-shoe nebula. This is a gaseous emission nebula and is located in the constellation of Sagittarius. The optically brightest portion of the nebula which is roughly rectangular in shape has been estimated to have a mass about 800 times that of the Sun.

4.8.3 Galactic Centre (Map 1)

From the time of Jansky's earliest measurements it was recognised that the most intense radio emission was received from the direction of the galactic center. High resolution observations by Downes and Maxwell (1966) revealed that the galactic center encompasses several discrete sources

surrounding the very intense Sagittarius- A source. In our map we see two peaks of maximum brightness to the north-east of the galactic centre and an absorption feature to the south west of the galactic centre.

4.8.4 Spurious Responses In The Map

4.8.4.1 Sidelobes

The maps presented here were made by using the fourier components measured by a set of discretely spaced interferometers. The level of the sidelobes depends upon the grading used for the measured fourier components. The maps presented here used a uniform weighting function which results in sidelobes as high as 21% of the main response. This naturally causes confusion when there are many sources in the sky. At decametric wavelengths, the sidelobes of strong sources like Cygnus, Cas A, Virgo and Crab do not permit high sensitivity observations in their vicinity. Map 9 shows the sidelobes due to Cygnus . The source Cygnus A is 32 minutes away in R-A and 11° away in declination from the centre of the map. Many deconvolution techniques have been developed recently to remove the undesirable effects caused by the sidelobes. However these techniques run into special problems when applied to large scale maps like the ones presented here which have both extended and point source emissions.

4.8.4.2 Interference

The sharp features in the maps 1,3 and 4 can be easily recongised to be non astronomical. These are due to man made interference, and can be excised by using software techniques.

4.9 LOW FREQUENCY RECOMBINATION LINE OBSERVATIONS

Shklovsky (1956) had predicted already in 1956 that electronic transitions between the hyperfine structure sublevels of atomic nitrogen should be observable in the decametre waveband. Peter Shaver (1975) showed that the possibility of observable recombination lines below 200 MHz is greatest for the case of negative absorption in low-density gas in front of strong radio sources. During the period from December 1976 to May 1979, Konovalenko and Sodin repeatedly endeavoured to detect lines in the range $H650\alpha$ -$H630\alpha$. The spectrum of cosmic radiowaves from the discrete sources Cassiopea A, Cygnus A and Taurus A were investigated. No hydrogen recombination lines of intensity above 3×10^{-3} of the background were detected below 27 MHz. In June 1978, they also attempted to detect the N14 absorption lines. They were successful in detecting a 26.13 MHz absorption line in the direction of Cas A which they attributed to the 26.127 MHz $F = 5/2 \longrightarrow 3/2$ hyperfine transition of 14N. In 1980, Blake, Crutcher and Watson pointed out that a unique line identification cannot be made on the basis of frequency alone. They argued that

Konovalenko and Sodin required an abundance ratio of $N/H = 8 \times 10^{-3}$ to explain the strength of the line observed. This ratio compared with the cosmic ratio of 1.2×10^{-4} was very high and would require a modification of the existing ideas about galactic nucleosynthesis. Blake et. al. therefore suggested that the line was the 631α recombination line due to neutral atoms of a heavy element, either carbon atoms in the HI clouds or possibly heavier atoms (Mg, Ca, Fe) in hot ionized gas along the line of sight. Later, Konovalenko and Sodin examined a series of spectra near the C630α line and concluded that the low frequency absorption line in the spectrum of Cas A was due to the presence of a cold cloud of ionized carbon.

With the installation of the DSB spectrometer at Gauribidanur, confirmation of the recombination line in the direction of Cas A and a search for low frequency recombination lines in the directions of Cygnus A, Taurus A and the galactic centre were attempted in September 1984. We were successful in detecting the C574α and C575α lines in the direction of Cas A. No lines with $T_L/T_C \geq .002$ were detected in the direction of Cygnus A (Figs 4.13 and 4.14). The Taurus A and the galactic centre observations were partly corrupted by interference, and in the short interference free periods available no lines were detectable.

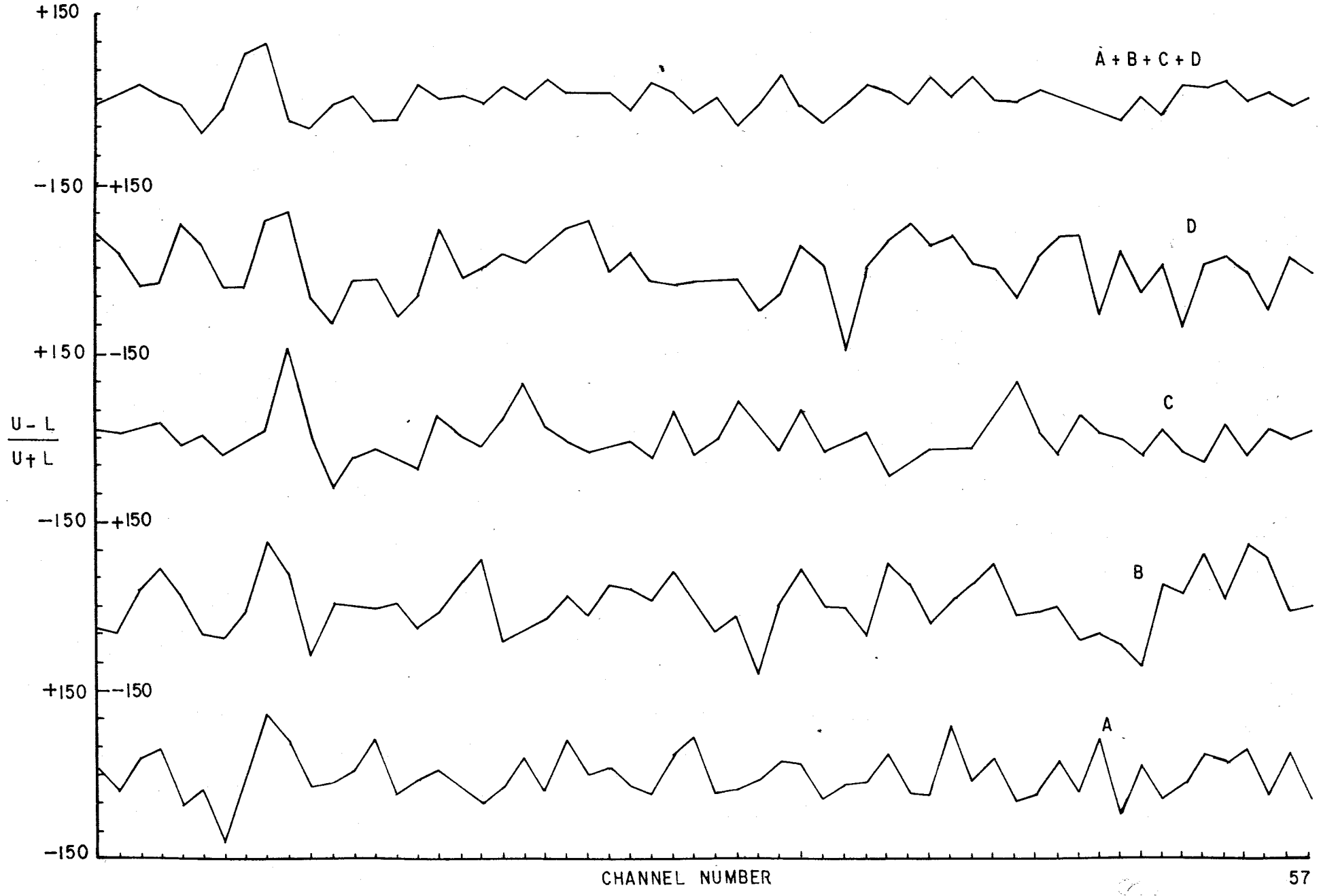

FIG. 4·13 OBSERVATION OF C574 α AND C575 α IN THE DIRECTION OF ~~CAS~~ A.

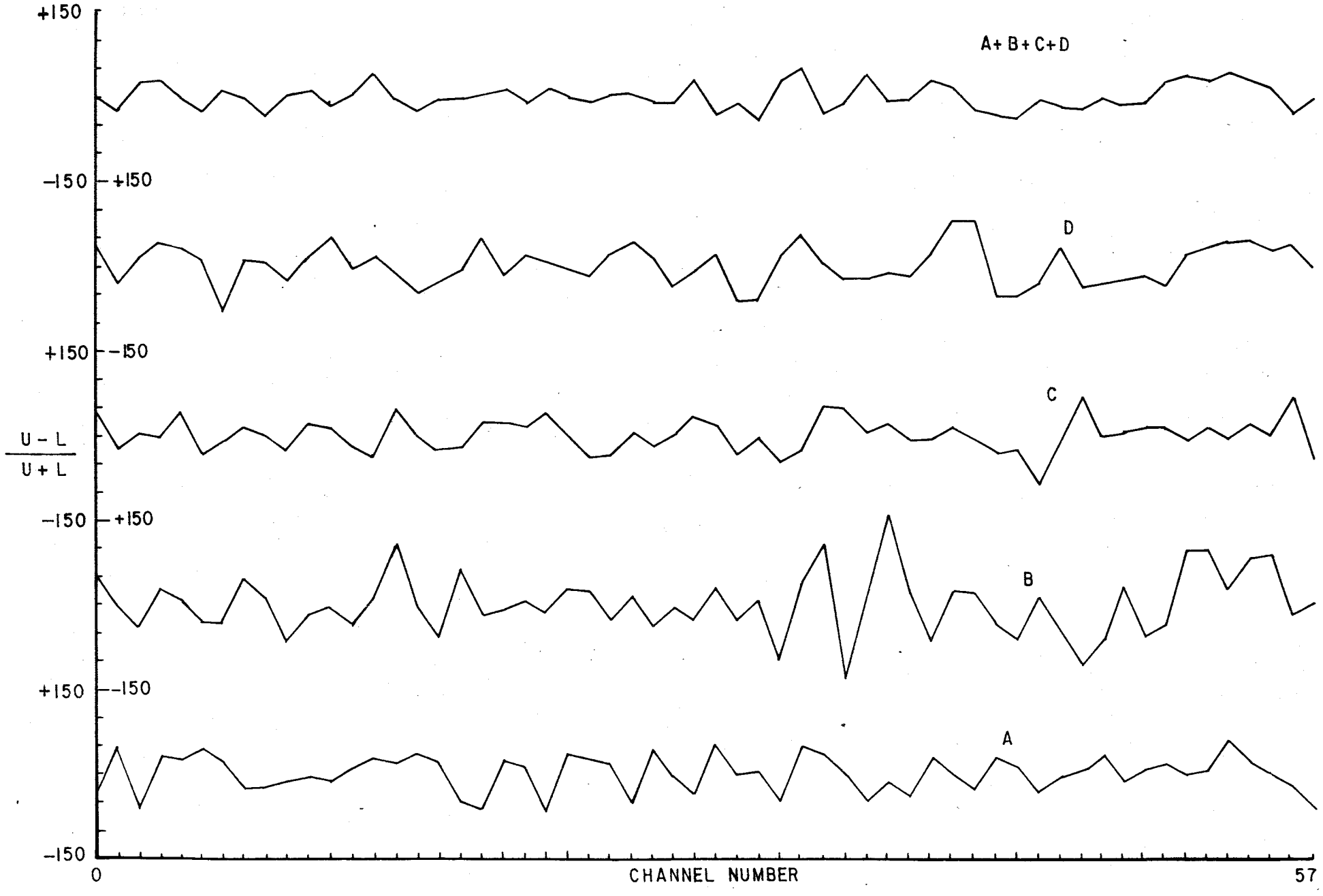

FIG. 4·14 OBSERVATION OF C574α AND C575α IN THE DIRECTION OF Cyg A.

4.9.1 Observational Procedure

The D.S.B. spectrometer is described in section 2.9. The N-S array was used for observation by phasing it to the source under consideration. The N-S array has less collecting area than the E-W array, but then observation time obtainable with the E-W array tracking and with the N-S array without tracking are comparable for these declinations. The N-S array was used for the observations since they would not involve the beam flipping required for tracking. This simplifies recording. The weighting scheme required in the data analysis is simpler when the N-S array is used. The L.O. used for observation was 34.629 MHz, and the sampling frequency was 333 KHz. These were carefully chosen to avoid any harmonic of the sampling frequency giving rise to an inband product. A.C. coupling was employed to attenuate frequencies very close to D.C.

Between the two possibilities of observing a single line with higher resolution or two lines with somewhat lower resolution the latter was preferred because

1. It gives a higher SNR and thus enables detection in a shorter time.

2. Interference can be ruled out beyond any doubt if two lines (one in the U.S.B., and one in L.S.B.) can be detected simultaneously.

With a pre integration time of around 1.5 secs, 128 cos and 128 sine correlation coefficients were recorded on magnetic tape. Post integration after recording and Fourier Transformation to obtain power spectra were done off-line at Bangalore. The cosine transform of the cos correlation coefficients gives the sum of the two R.F. sidebands and thus the video bandshape. The Sine transform of the sine correlation gives the difference between the two R.F. sidebands. The spectrum of Cas A, Cyg A are shown in Figures 4.13 and 4.14.

1. Each spectrum shown is the unsmoothed raw spectrum. No baseline is removed. Such an excellent baseline is simply due to the final video bandwidth being a very small fraction of the R.F. bandwidth.

2. The observation was repeated with a shifted L.O. to rule out interference.

3. During these observations, the system temperature was dominated by Cas A and Cyg A. The observed line strength and optical depth are related by

$$\tau = \tau_{Measured} \left(1 + T_B / T_S \right)$$

T_B and T_S are the antenna temperatures due to the background and the source. Since T_S changes during the observations, it is not appropriate to give equal weightage to the entire observation.

Each observational point should get a weighting proportional to the strength of the source in the beam at that time. Appendix C describes a simple weighting scheme which can be used.

4. As mentioned earlier the sine transform of the sine correlation gives the difference between the two sidebands. Whether it is U.S.B. - L.S.B. or L.S.B. - U.S.B. depends on which of the L.Os. is leading and which way the sine correlation is measured. To check the assignment of sidebands a strong C.W. was added to the antenna noise after the observation and the difference and the sum spectra were obtained. Figs 4.13 and 4.14 show the spectra before checking the assignment of sidebands.

5. The variation of U + L over the day was found to be very small. This indicated that one need not measure U + L all the time and all the 256 correlators can be used to measure U - L. This increases the much needed resolution at these frequencies. U + L can be measured before and after the observation with the same resolution.

6. Another important requirement for a sensitive observation of this type is proper functioning of the correlators. Actually it was found that some correlator channels which functioned very well for short integration times, showed unacceptable deviations from the expected behaviour over long integration times. Most of these bad correlators were set right by changing a few counter chips

in the correlators which might have malfunctioned intermittently.

4.10 DISCUSSION

A single absorption feature was detected in the spectrum of Cas A (Fig 4.15) at a velocity of 50kms/s. (T_L / T_c = .002) The velocity corresponds to that of the deepest known 21 cm absorption due to a single HI cloud. As mentioned earlier, Blake had pointed out that it is most likely that the line is due to carbon if originating in cold gas. It could also be due to heavier elements such as Ca or Mg if located in hot gas. The agreement in velocity in our observation with the HI absorption feature strongly favours cold dense HI clouds as the site of absorption and carbon as the element in question. A similar optical depth was obtained by K.R. Anantharamaiah et.al. (1985) in their observations at Green Bank at 25, 38, 52 and 68 MHz. Apart from the confirmation of the low frequency recombination line they were looking for "The turnover phenomenon" of optical depth. All high frequency observations show recombination lines of hydrogen or heavier elements only in emission. Thus the C line which is seen in absorption below 38 MHz should be seen in emission at some higher frequency, i.e., the optical depth should go through zero and change sign. This phenomena has not been observed yet, but in any case, such an investigation is not possible in Gauribidanur now as the Receiver System can only be tuned within a 2 MHz

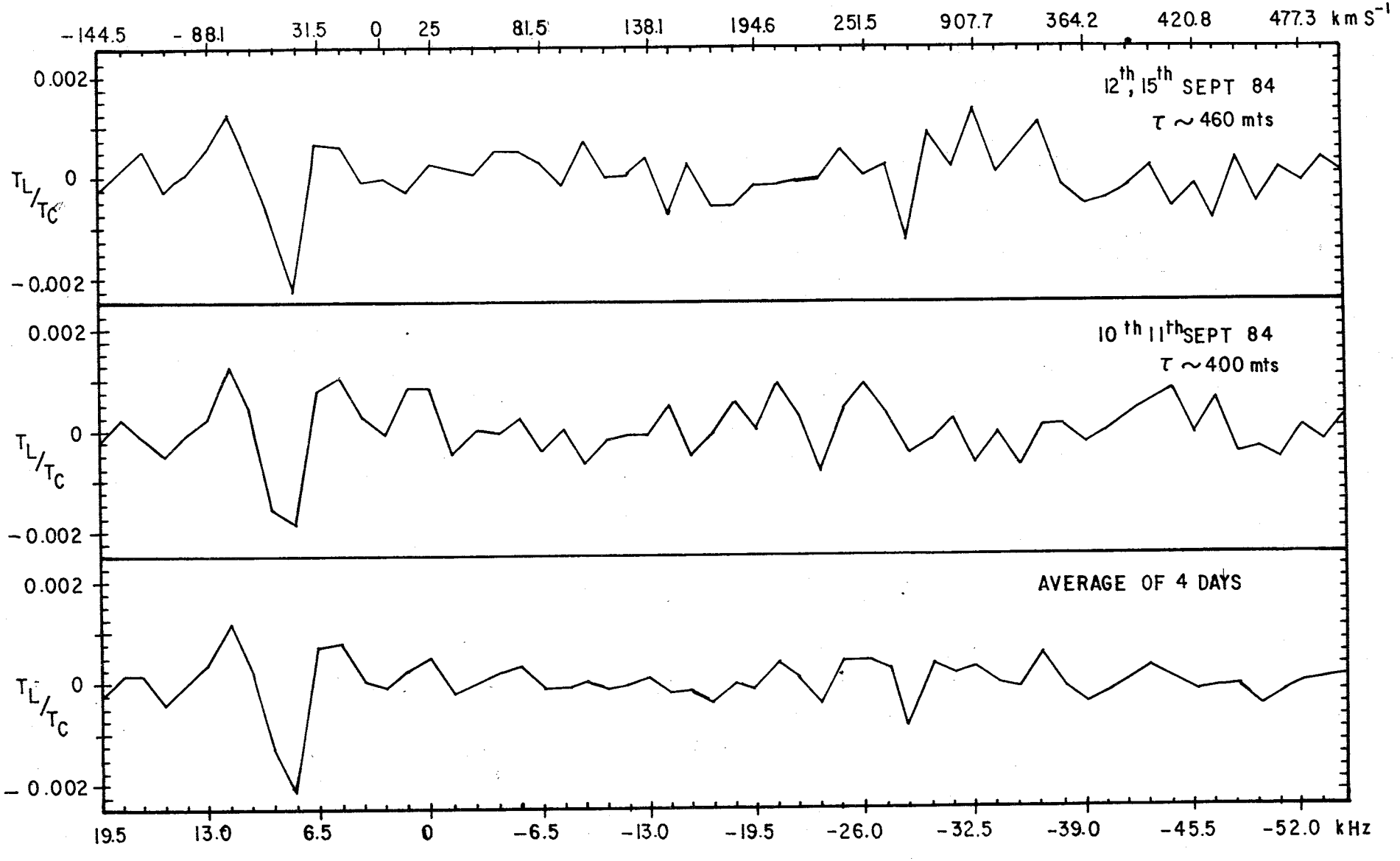

FIG.4·15 OBSERVATION OF C574α AND C575α IN THE DIRECTION OF CAS A.

band around 34.5 MHz.

A broad band antenna (30 to 80 MHz) is presently being installed at Gauribidanur for solar work. Its effective collecting area and integration time available per day promise the possibility of a low frequency recombination survey of the galactic plane using the existing receiver system.

Note: The observed profile will be centred around the expected line frequency if the intervening cloud is stationary. If the cloud is moving the profile would be displaced. The frequency shift $\Delta\nu$ and the velocity of the cloud are related by

$$\Delta\nu/\nu = V/C$$

V = velocity of approach (-) or recession (+)

C = velocity of light

$\Delta\nu$ = frequency shift

ν = rest frequency

At the observing frequency of C574$\propto$ a frequency shift of 1 KHz corresponds to a velocity of 8.66 Kms . In radio astronomy it is a common practice to use the velocity as the abscissa for plotting the line profiles.